Nuclear movement regulated by non-Smad Nodal signaling via JNK is associated with Smad signaling during zebrafish endoderm specification

Shunya Hozumi, Shun Aoki, and Yutaka Kikuchi*

Department of Biological Science, Graduate School of Science, Hiroshima University, Kagamiyama 1-3-1, Higashi-Hiroshima, Hiroshima, 739-8526 Japan

*Corresponding Author: Yutaka Kikuchi (E-mail yutaka@hiroshima-u.ac.jp)

Keywords nuclear movement; endoderm specification; Nodal; Smad; JNK; MTOC

SUMMARY STATEMENT

In zebrafish embryos, nuclear movement occurs in the first endoderm cells. This process is regulated by non-Smad JNK downstream of Nodal, and is associate with Smad signaling toward the nucleus.

ABSTRACT

Although asymmetric nuclear positioning is observed during animal development, the regulation and significance of this nuclear positioning in cell differentiation remains poorly understood. Using zebrafish blastulae, we provide evidence that nuclear movement toward the yolk syncytial layer, which comprises extraembryonic tissue, occurs in the first endoderm specified cells during endoderm specification. Nodal signaling is essential for nuclear movement, whereas nuclear envelope proteins are involved in the movement through the microtubule formation. The positioning of the microtubule organizing center, which is proposed to be critical for nuclear movement, is regulated by Nodal signaling and nuclear envelope proteins. The non-Smad JNK signaling pathway, which is downstream of Nodal signaling, regulates nuclear movement independent of the Smad pathway, and this nuclear movement is associated with Smad signal transduction toward the nucleus. Our study provides insights into the function of nuclear movement in Smad signaling toward the nucleus, and could be applied to the control of Transforming Growth Factor-β signaling.

INTRODUCTION

The largest organelle, the nucleus, is not always located in the center of the cell. Asymmetrical positioning of the nucleus has been observed in differentiated animal cells and tissues, including skeletal muscles, many epithelial cells, and neurons (Dupin and Etienne-Manneville, 2011, Gundersen and Worman, 2013). Abnormal positioning leads to cellular dysfunction and diseases, such as muscular dystrophy, cardiomyopathy, and lissencephaly (Gundersen and Worman, 2013, Bone and Starr, 2016). The positioning of the nucleus is dynamically regulated during cell division and migration (Dupin and Etienne-Manneville, 2011, Gundersen and Worman, 2013). Recent studies revealed that nuclear positioning is controlled by microtubules (MTs), actins, and associated motor proteins. In addition, the linker of nucleoskeleton and cytoskeleton (LINC) complex, which is composed of outer nuclear membrane KASH-domain (Klarsicht, Anc1, and Syne homology) proteins and inner nuclear membrane SUN-domain (Sad1 and Unc-83) proteins (Bone and Starr, 2016, Dupin and Etienne-Manneville, 2011, Gundersen and Worman, 2013), has also been shown to be involved in nuclear positioning. It has been suggested that the position of the microtubule organizing center (MTOC) and the connection between the MTOC and the nucleus are crucial for MT-mediated nuclear movement (Bone and Starr, 2016, Gundersen and Worman, 2013). While many studies have suggested that nuclear positioning plays an important role in cellular function, only one study has reported on the relationship between nuclear positioning, asymmetric signaling, and cell fate determination (Del Bene et al., 2008, Gundersen and Worman, 2013). In the developing zebrafish retina

neuroepithelium, nuclear movement, termed interkinetic nuclear migration (INM), is correlated with cell cycle exit and Notch signaling activation; this process is regulated by Syne (LINC complex protein) and the motor protein dynactin 1 (Del Bene et al., 2008, Gundersen and Worman, 2013). However, the exact mechanisms of nuclear movement, and the relationship between nuclear movement and cell fate determination, remain to be elucidated.

Nodal, a transforming growth factor (TGF)-β superfamily member, is a ligand that regulates the expression of its target genes by binding to their receptors and inducing the phosphorylation of Smad2/3 (Di Guglielmo et al., 2003, Penheiter et al., 2002, Hayes et al., 2002). In mouse and zebrafish embryos, Nodal is essential for mesendoderm induction prior to gastrulation (Weinstein et al., 1998, Nomura and Li, 1998, Jia et al., 2008). Genetic analyses in zebrafish revealed that two *Nodal*-related genes, *Nodal-related 1* (*ndr1*) and *Nodal-related 2* (*ndr2*), are essential, and EGF-CFC family gene *teratocarcinoma-derived growth factor 1* (*tdgf1*), a co-receptor of Nodal, is necessary for mesendoderm induction (Schier, 2009). In addition, analyses using various zebrafish mutants and knockdown experiments have identified molecular pathways leading to the endoderm cell fate (Fukuda and Kikuchi, 2005, Zorn and Wells, 2009). It has been shown that Sox32/Casanova is an essential transcription factor for endoderm fate determination downstream of Nodal/Smad signaling (Dickmeis et al., 2001, Kikuchi et al., 2001). Aside from the Smad-pathway, TGF-β also activates non-Smad signaling pathways, such as extracellular signal-regulated kinase (Erk), p38, and c-Jun N-terminal kinase (JNK) (Moustakas and Heldin, 2005, Derynck

and Zhang, 2003, Mu et al., 2012). Smad and non-Smad signaling pathways are involved in the regulation of various cellular processes, including cell differentiation, proliferation, migration, epithelial-mesenchymal transition (EMT) through cell context-dependent transcription, and regulation of cytoskeleton and cell junction formation (Moustakas and Heldin, 2005, Derynck and Zhang, 2003, Mu et al., 2012); however, the interactions between these pathways are poorly understood.

During the course of our analysis of endoderm specification, we discovered distinct nuclear movement toward the yolk syncytial layer (YSL) in the most laterally located marginal cells (LMCs), which are the first cells fated to differentiate into the endoderm. In this study, we explored the regulation and significance of nuclear movement in LMCs by Nodal signaling, and identified that the non-Smad JNK signaling pathway regulates nuclear movement independent of Smad; this movement leads to transduction of the Smad signal toward the nucleus.

RESULTS

Nodal signaling is necessary for nuclear movement toward the YSL in the most laterally located marginal cells during endoderm specification

In order to explore the process of endodermal fate determination from the sphere (4.0 hours post fertilization: 4.0 hpf) to the late blastula stage (4.7 hpf), we carefully observed the spatiotemporal emergence and distribution of *sox32*-expressing endoderm cells in the marginal domain of wild-type (WT) embryos using fluorescence *in situ* hybridization (FISH). Expression of *sox32* was first detected in LMCs located adjacent to both the YSL and the enveloping layer (EVL) cells (Figure 1A; cell shown in green). At 4.7 hpf, 97.7 % (43/44) of LMCs were *sox32*-positive (Figures 1B and B'; arrowheads). In contrast, medial marginal cells (MMCs, Figure 1A; cells shown in red), which were adjacent to both LMCs and the YSL, did not express *sox32* at 4.7 hpf (2.3 % [1/44] of MMCs were *sox32*-positive; Figures 1B and B'; arrows), indicating that LMCs are the first endoderm specifying cells in zebrafish embryos. We found that nuclear positioning of LMCs in WT embryos at 4.7 hpf appeared to be closer to the YSL as compared with that in WT embryos at 4.0 hpf (Figure 1B, B' and D; arrowheads). In addition, nuclear positioning of LMCs appeared to be more distant from the YSL following treatment with TGF-β type I receptor inhibitors, SB505124 or SB431542 (Laping et al., 2002, Inman et al., 2002, Callahan et al., 2002, DaCosta Byfield et al., 2004), at 4.7 hpf (Figures 1E and F; arrowheads). This suggests that Nodal signaling is involved in determination of nuclear positioning in LMCs. We next performed confocal time-lapse analysis to visualize the positional change of nuclei in LMCs and MMCs. The

time-lapse images clearly showed that while the nuclei in both LMC and MMC moved toward the YSL, the nucleus in LMC was closer in proximity to the YSL as compared with that in MMC between 4.0 and 4.7 hpf (Movies S1 and S2).

In order to evaluate nuclear movements during endoderm specification, we measured the minimum distance between the most vegetal position of the nucleus and the blastoderm/YSL boundary (DNB) (Figure 1G). The mean DNB value in LMCs of WT embryos was significantly reduced from 4.10 μm at 4.0 hpf to 1.75 μm at 4.7 hpf; this reduction was blocked by treatment with SB505124 or SB431542 (Figure 1G). We also investigated the positional change of nuclei in MMCs (Figure 1A) at 4.7 hpf. The mean DNB value in MMCs at 4.7 hpf was slightly, but significantly, lower than that at 4.0 hpf, whereas at 4.7 hpf, the mean DNB value in LMCs was significantly lower than that in MMCs (Figure 1G). We also explored the minimum distance between the center of the cell and the most vegetal position of nucleus (DCN) (Figure 1H). We did not detect any marked differences between DNB and DCN values in the positional change of nuclei in LMCs and MMCs (Figures 1G and H). We next examined the nuclear positioning of LMCs and MMCs relative to the center of the cells (Figure S1). Our results indicated that 57 % of nuclei in LMCs at 4.0 hpf were localized between zero and approximately +90 degrees. At 4.7 hpf, 67 % of LMCs had shifted to between zero and approximately -90 degrees (Figure S1). More than 50 % of the nuclei in MMCs of WT embryos and in LMCs of SB505124- or SB431542-treated embryos maintained their positions at 4.7 hpf (Figure S1). These results showed that nuclei

of LMCs in WT embryos moved toward the YSL between 4.0 and 4.7 hpf and that Nodal signaling is necessary for this nuclear movement.

We and others have previously shown that both Mixl1 and Gata5 are necessary for endoderm specification downstream of Nodal signaling and upstream of Sox32 (Fukuda and Kikuchi, 2005, Zorn and Wells, 2009). We examined *mixl1* and *gata5* expression at 4.7 hpf, and found that *mixl1* was widely expressed in marginal cells, whereas *gata5* expression was restricted to the LMCs (Figure 1I). Consistent with previous results, *sox32* expression was only detected in LMCs, along with *mixl1* and *gata5* (Figure 1I). In addition, at late blastula stage, expression of *gata5* was restricted to the mesendoderm, which is a region comprising three to four rows of cells from the margin (Alexander et al., 1999, Rodaway et al., 1999, Ober et al., 2003), suggesting that high Nodal signaling is necessary for *gata5* expression. To confirm that Nodal signaling is highly activated only in the nucleus of LMCs at 4.7 hpf, we used an antibody for phosphorylated Smad2 (p-Smad2), a downstream effector of Nodal signaling. A previous report showed that the overexpression of mutated Smad2/3 phosphorylation sites repressed mesendoderm induction in zebrafish embryos (Jia et al., 2008), suggesting that p-Smad2 plays a significant role in endoderm specification. Both p-Smad2 protein and *sox32* mRNA were detected only in the nuclei of LMCs at 4.7 hpf, but not at 4.0 hpf (Figure 1J). These results indicate that p-Smad2 nuclear translocation, which leads to *sox32* induction, is associated with nuclear movement toward the YSL in LMCs.

Enhancement of Nodal signaling in the YSL induces nuclear movement in MMCs toward the YSL

Having shown that nuclear movement of LMCs requires Nodal signaling during endoderm specification, we then wanted to confirm whether Nodal overexpression induces nuclear movement in MMCs toward the YSL. To address this question, *ndr1* mRNA, together with dextran-Alexa Fluor® 594, was injected into the YSL at 3.0 hpf (Figure 2A). Fluorescence was only observed in the YSL due to the lack of permeability between the blastoderm and the YSL (Figures 2C and C'; white brackets); this was consistent with previous results (Gritsman et al., 1999). Mean DNB and DCN values in MMCs of WT embryos were reduced from 3.30 μm to 1.12 μm and from -4.53 μm to -5.45 μm, respectively, at 4.7 hpf, when *ndr1*-mRNA was overexpressed in the YSL (*ndr1* mRNA>YSL) (Figures 2B-E). In addition, nuclear positioning in MMCs was located between zero and approximately +90 degrees (48 %) in WT embryos (Figure 2F). On the other hand, 76 % of nuclei in MMCs was located between zero and approximately -90 degrees in *ndr1* mRNA>YSL embryos (Figure 2E), similar to those observed in the nuclei of LMCs at 4.7 hpf (Figure S1). Therefore, Nodal signaling has the ability to induce nuclear movement not only in LMCs, but also in MMCs.

Functional inhibition of LINC complex proteins blocks nuclear movement in LMCs, probably through MTOC attachment to the nucleus and MT formation

Previous reports indicated that the KASH domain, a component of the LINC complex proteins, is required for nuclear migration in *Drosophila* and *C. elegans* (Bone and Starr, 2016, Dupin and Etienne-Manneville, 2011, Gundersen and Worman, 2013). Overexpression experiments using a KASH domain of Syne2a (C-Syne2a), which functions as a dominant negative form of this protein, showed that positioning of cell nuclei in zebrafish photoreceptors is dependent on the *syne* gene family (Tsujikawa et al., 2007). These results prompted us to analyze the function of LINC complex proteins in endoderm specification and nuclear movement of LMCs by using the C-Syne2a (Tsujikawa et al., 2007). We first monitored the effect of *C-syne2a* mRNA overexpression on endoderm specification using the endoderm marker *sox32*. Whole-mount *in situ* hybridization (WISH) and quantitative PCR (qPCR) analyses indicated that expression of both *sox32* and the mesodermal marker *T, brachyury homolog a* (*ta*) was significantly reduced in *C-syne2a*-overexpressing embryos compared with that in *nuclear lacZ* (*nlacZ*)-overexpressing embryos at 5.3 hpf without affecting the expression of *ndr1* and *ndr2* (Figure S2). The mean DNB and DCN values of LMCs in WT embryos were 2.13 μm and -5.93 μm, respectively, at 4.7 hpf, whereas those of *C-syne2a*-overexpressing embryos were 4.24 μm and -3.51 μm (Figures 3A-D). At 4.7 hpf, 58 % of nuclei in LMCs of *C-syne2a*-overexpressing embryos were localized between zero and +90 degrees (Figure 3E),

similar to observations of LMC nuclei at 4.0 hpf (Figure S1). Therefore, overexpression of *C-syne2a* resulted in the inhibition of nuclear movement toward the YSL in LMCs. In addition, while *sox32*-expressing nuclei in LMCs were p-Smad2-positive in WT embryos, both *sox32* and p-Smad2 protein expressions were negative in LMCs of *C-syne2a*-overexpressing embryos at 4.7 hpf (Figure 3F). These results suggest that LINC complex proteins regulate both nuclear movement and p-Smad2 nuclear translocation in LMCs to induce endoderm specification.

LINC complex proteins are known to mediate the connection between the nuclear envelope and components of the cytoskeleton (MTs and actin filaments)/microtubule-organizing centers (MTOCs) (Bone and Starr, 2016, Gundersen and Worman, 2013). It has been shown that nuclear attachment to MTOCs is required for pronuclear migration in *C. elegans* zygotes, and nuclear migration in *Drosophila* photoreceptor cells (Bone and Starr, 2016, Gundersen and Worman, 2013). Based on these previous results, we examined the positioning and formation of MTOCs and MTs in *C-syne2a*-overexpressing embryos. In WT embryos, two MTOCs were attached to the nucleus at 4.7 hpf, whereas the MTOCs in approximately 50 % of *C-syne2a*-overexpressing embryos were detached from the nucleus (Figures 3G-I). Furthermore, MT formation in LMCs of *C-syne2a*-overexpressing embryos was significantly reduced, but was higher than that of nocodazole-treated embryos (Figures 3J-M). This may be due to the abnormal positioning of MTOCs. Our results suggest that attachment of MTOCs to the nucleus is critical for nuclear movement via MT formation in LMCs.

Nuclear movement and MTOC positioning are regulated by the Nodal/JNK signaling pathway

C-syne2a-overexpression experiments suggested that the positioning of MTOCs and MT formation are involved in nuclear movement of LMCs during endoderm specification. In order to evaluate the positioning of MTOCs during endoderm specification, we calculated the following parameters (Figure 4A): the minimum distance between the most vegetal position of MTOCs and the blastoderm/YSL boundary (a); the length of the LMCs (b). The a/b ratio was significantly reduced from 0.36 at 4.0 hpf to 0.23 at 4.7 hpf, whereas treatment with the TGF-β inhibitor (SB505124 or SB431542) prevented this change in the ratio between 4.0 and 4.7 hpf (Figures 4B-E and H). These results showed that MTOCs are reoriented to a position closer to the YSL during endoderm specification, and that Nodal signaling regulates this process.

Various chemical inhibitors that block downstream signaling pathways of TGF-β were used to determine the regulatory mechanisms of MTOC reorientation by Nodal signaling. Specific inhibitors included NSC23766 (a Rac1 inhibitor) (Gao et al., 2004), Y27632 (a Rock inhibitor) (Han et al., 2001), ML141 (a Cdc42 inhibitor), LY294002 (a phosphoinositide 3-kinase inhibitor) (Vlahos et al., 1994), SB203580 (a p38 MAP kinase inhibitor) (Cuenda et al., 1995), NF-κB activation inhibitor (a nuclear factor-kappa B inhibitor) (Tobe et al., 2003), and SP600125 (a c-Jun N-terminal kinase (JNK) inhibitor) (Bennett et al., 2001). WISH and qPCR showed that expression of both *sox32* and *ta* was significantly down-regulated by

JNK inhibitor (SP600125) at 4.7 hpf without affecting the expression of *ndr1* and *ndr2* (Figure S3).

We next examined MTOC reorientation, nuclear movement, MT formation, and nuclear translocation of p-Smad2 in JNK signaling-inhibited embryos. Both MTOC reorientation and nuclear movement were significantly inhibited by the two JNK inhibitors used (SP600125 and EMD 420123), when assessed at 4.7 hpf (Figures 4F-H and 5A-E). Unlike the *C-syne2a*-overexpressing embryos, MT formation was not affected by treatment with either SB505124 or SP600125 at 4.7 hpf (Figure S4). In addition, nuclear translocation of p-Smad2 was not detected in LMCs when JNK signaling was inhibited (Figure 5F). We further observed the presence of phosphorylated JNK (p-JNK), an activated form, in the LMC/YSL boundary at 4.7 hpf (Figure 6). The p-JNK signals in the boundary were significantly reduced in SB505124-treated embryos at 4.7 hpf (Figure 6). These results suggest that MTOC reorientation, nuclear movement, and nuclear translocation of p-Smad2, all of which induce endoderm specification in LMCs, are regulated by JNK signaling downstream of Nodal in YSL.

Non-Smad JNK signaling regulates nuclear movement independent of the Smad2 pathway

It is well known that Smad and non-Smad pathways, including JNK signaling, are downstream of TGF-β (Derynck and Zhang, 2003, Moustakas and Heldin, 2005, Mu et al., 2012). We overexpressed *ndr1* in the YSL (*ndr1* mRNA>YSL) of SP600125-treated

embryos in order to analyze the relationship between these two signaling pathways. Interestingly, *sox32* expression in MMCs was not observed in *ndr1* mRNA>YSL embryos treated with SP600125 at 4.7 hpf (Figures 7A-B'). In addition, mean DNB and DCN values in MMCs were not reduced in SP600125-treated embryos as compared with those in DMSO-treated embryos, despite *ndr1* mRNA overexpression in the YSL (Figures 7C, D).

We next investigated the hierarchical relationship between Smad and non-Smad JNK signaling pathways with respect to nuclear movement via a dominant-negative form of Smad2 (dn smad2), which is mutated in the C-terminus phosphorylation sites by receptor tyrosine kinases (Jia et al., 2008). A previous study reported that overexpression of *dn smad2* mRNA abolishes *sox32* induction by ectopic Nodal signaling in zebrafish embryos (Jia et al., 2008). Similarly, we found that *sox32* expression was significantly reduced in *dn smad2*-overexpressed embryos (Figures 7E-G). In addition, nuclear movement in *dn smad2*-overexpressed embryos was unchanged compared with that in *nlacZ*-overexpressed embryos (Figures 7H-K), further confirming that nuclear movement regulated by non-Smad JNK signaling is independent of Smad signaling pathway.

Nuclear movement toward the YSL is associated with nuclear translocation of Smad2

As nuclear movement toward the YSL results in p-Smad2 nuclear translocation during zebrafish endoderm specification (Figures 1J, 3F, and 5F), we hypothesized that nuclear Smad2 increases in proportion due to nuclear movement toward the YSL. We visualized Smad2 nuclear translocation using time-lapse confocal live imaging in zebrafish embryos, as

previously reported (Harvey and Smith, 2009, Dubrulle et al., 2015). We co-injected *EGFP-smad2*, *smad4a*, *membrane bound* (*mb*)-*RFP*, and *H2B-mCherry* mRNAs at the one cell stage, then injected *nlacZ* or *ndr1* mRNA with dextran-Alexa Fluor® 594 into the YSL at 3 hpf; EGFP-Smad2 fluorescence was observed in MMCs at 5.3 - 6.0 hpf (Figure S5). The nuclear/cytoplasmic ratio of EGFP-Smad2 fluorescence gradually increased as the nucleus moved toward the YSL when *ndr1*, but not *nlacZ*, mRNA was injected into the YSL (Figures 8A-C). Our results suggest that nuclear movement toward the YSL is associated with Smad2 nuclear translocation.

DISCUSSION

A model of the Nodal signaling pathway leading to endoderm specification

It is well known that induction of both endoderm and mesoderm in early vertebrate development is regulated by Nodal-Smad2/3 signaling pathways (Schier, 2009). The endoderm and mesoderm may arise from single marginal cells in zebrafish embryos at the blastula stage; it appears that the fate of marginal cells is determined by the strength of Nodal signaling (Fukuda and Kikuchi, 2005, Zorn and Wells, 2009). However, regulation of Nodal signaling strength in the marginal cells has not yet been fully elucidated. In this study, we arrived at four conclusions. First, Nodal signaling is essential for nuclear movement toward the YSL, whereas nuclear envelope proteins are involved in this movement through microtubule formation. Second, positioning of the MTOC is regulated by Nodal signaling and nuclear envelope proteins. Third, the non-Smad JNK signaling pathway, which acts

downstream of Nodal signaling, regulates nuclear movement independent of Smad2. Fourth, this nuclear movement is associated with Smad signal transduction toward the nucleus. Based on our results, we proposed a model for signal transduction pathways that resulted in endoderm specification of LMCs (Figure 9): Nodal activates two signaling pathways: Smad2- and JNK-mediated signaling. Activation of JNK, which is a different pathway from phosphorylation of Smad, induces nuclear movement toward the YSL and MTOC reorientation is involved in this movement. This nuclear movement mediates the nuclear translocation of p-Smad2 into the nucleus, which then initiates the molecular programs for endoderm specification. Finally, activation of *sox32* drives cellular fate toward endoderm differentiation. In our model, Nodal signaling should be higher in LMCs than in other marginal cells between 4.0 and 4.7 hpf, since nuclear movement occurs in LMCs at 4.7 hpf. Consistent with this idea, we found that *gata5* and *sox32* expression, which are thought to be activated by high Nodal signaling (Alexander et al., 1999, Rodaway et al., 1999, Ober et al., 2003), were restricted to the LMCs at 4.7 hpf (Figure 1H).

It is well analyzed that mitogen-activated protein kinases (MAPKs), a family of serine/threonine protein kinases, are part of the downstream signaling of TGF-β, and consist of three subgroups: Erk, p38, and JNK. Previous studies have revealed that MAPKs phosphorylate the linker region of Smad2/3 by activation of TGF-β, which, in turn, blocks the nuclear translocation of Smad2/3 (Massague, 2003, Mori et al., 2004, Wrighton et al., 2009). In *Xenopus* embryos, overexpression of Smad2 with a mutation in the linker region of phosphorylation sites leads to nuclear accumulation of the mutated Smad2. This prolongs

the response time of endogenous mesodermal genes to activin signaling (Grimm and Gurdon, 2002). In zebrafish embryos, overexpression of Smad2 mutants results in an increase in mesoderm and endoderm genes (Liu et al., 2013), suggesting the inhibitory function of Smad2 phosphorylation by MAPKs. On the other hand, we showed that inhibition of JNK by SP600125 resulted in a reduction of *sox32* expression (Figure S3). Therefore, JNK does not seem to be involved in endoderm gene induction via direct phosphorylation of the linker region of Smad2. Similar to endoderm maker *sox32*, the expression level of a mesoderm marker gene, *ta*, was significantly reduced in JNK-inhibited and *C-syne2a*-overexpressing embryos (Figures S2 and S3). However, since *ta* expression was down-regulated only in the dorsal side of Nodal signaling-deficient embryos (Feldman et al., 1998, Gritsman et al., 1999), it is possible that JNK and nuclear envelope proteins regulate *ta* expression via Nodal-independent signaling pathway.

Thus far, only one study has reported on the relationship between nuclear positioning and asymmetric signaling in the zebrafish retinal neuroepithelium (Del Bene et al., 2008). This report showed that during INM, the strength of Notch signaling is dependent on nuclear movement along the apical-basal axis of the neuroepithelium in radial glia cells (Del Bene et al., 2008). Consistent with their results, expressions of *notch1a* and *deltab/c* were found to be higher at the apical and basal surfaces of the retina, respectively (Del Bene et al., 2008). On the other hand, we showed that both Smad and non-Smad signaling pathways, cooperatively but independently, determine the specification of endoderm fate in zebrafish

blastulae. Our model provides a new system of signaling transduction downstream of TGF-β, which is associated with nuclear movement.

Nuclear movement by cytoskeletal components

Nuclear movement is mainly controlled by cytoskeletal elements (MTs and actin microfilaments) and associated motor proteins (Bone and Starr, 2016, Gundersen and Worman, 2013, Dupin and Etienne-Manneville, 2011). It has been reported that actin microfilaments and acto-myosin contraction are involved in nuclear movement, e.g. in cultured migrating fibroblasts and radial migration of neural precursors, mainly through pushing forces (Gundersen and Worman, 2013, Dupin and Etienne-Manneville, 2011). Based on these previous reports, we examined F-actin formation in WT and Nodal signaling-deficient embryos via phalloidin staining at 4.7 hpf. However, no obvious differences in F-actin formation were observed (Figure 6). In addition, inhibition of RhoA, Rac1, and Cdc24, which function as regulators of actin dynamics downstream of TGF-β signaling (Moustakas and Heldin, 2005, Derynck and Zhang, 2003, Mu et al., 2012), had no effect on endoderm specification (data not shown). These results suggest that nuclear movement in zebrafish LMCs during endoderm specification is an actin-independent process.

Our results indicated that overexpression of the dominant negative form of Syne2a inhibits nuclear movement. In addition, Syne2a regulates the attachment of MTOCs to the nucleus, and it necessary for MT formation in LMCs, suggesting that LINC complex proteins are involved in nuclear positioning via regulation of MT formation. In zebrafish

photoreceptors, nuclear movement is regulated by the motor protein dynein complex via MTs, and results in differential activation of Notch signaling along an apical-basal signaling gradient (Del Bene et al., 2008). However, it has recently been proposed that the Nodal signaling pathway is mediated through endocytosis. The zebrafish Rab5ab, a member of the RAB family of small GTPases, has been identified as an essential factor for Nodal signaling (Kenyon et al., 2015). Furthermore, MTs and associated motor proteins are necessary for the transportation of cellular components, including endocytic vesicles and organelles. Therefore, we did not analyze the function of motor proteins in the nuclear movement of LMCs, as it is difficult to exclude the possibility that inhibition of motor proteins, such as dynein and kinesin, affects endocytic vesicle-mediated Nodal signaling.

MTOC reorientation and nuclear movement are regulated by the JNK signaling pathway

The significance of MTOC positioning in nuclear movement has been investigated in several studies: male and female pronuclei migration in newly fertilized *C. elegans* eggs, oocyte migration in the *Drosophila* egg chamber, and INM in the vertebrate neuroepithelium (Gundersen and Worman, 2013, Starr, 2009). These studies revealed that the connection between the nucleus and MTs is mediated by LINC complex proteins, and that MTOC positioning appears to be a crucial factor in MT-mediated nuclear movement. In this study, we showed that one of the MTOCs in LMCs shifted closer to the YSL during endoderm specification (Figure 4). In addition, both MTOC reorientation and nuclear movement were

blocked when JNK signaling was inhibited (Figures 4 and 5). Our data, in combination with previous results, suggest that nuclear movement toward the YSL is elicited by the reorientation of the MTOC toward the YSL.

Immunological synapse formation between a T cell and an antigen-presenting cell is associated with MTOC reorientation, and novel and atypical members of protein kinase C family are involved in MTOC reorientation of T cells (Huse, 2012). In natural killer (NK) cells, on the other hand, JNK activation is required for NK cell cytotoxicity through MTOC reorientation (Li et al., 2008), suggesting that MAPKs are associated with MTOC reorientation. We have already shown that the Fgf/Mek/Erk signaling pathway negatively and positively regulates endoderm and mesoderm formation, respectively (Mizoguchi et al., 2006), suggesting that the Mek/Erk signaling pathway is not involved in the reorientation of MTOCs. In this study, we found that inhibition of p38 has no effect on endoderm specification (data not shown), and that Nodal-induced JNK activation regulates MTOC reorientation. However, further studies are required to elucidate the mechanism by which Nodal/JNK signaling regulates MTOC reorientation, which in turn contributes to nuclear movement.

MATERIALS AND METHODS

Zebrafish husbandry and drug treatments

All zebrafish experiments were approved by the Hiroshima University Animal Research Committee (Permit Number: F16-1). Wild-type (WT) AB strain zebrafish embryos were incubated in 1/3 Ringer's solution at 28.5°C (Mizoguchi et al., 2006) and staged according to the previous report (Kimmel et al., 1995).

Drug treatments

WT zebrafish embryos were dechorionated with 0.2 mg/ml pronase (Sigma-Aldrich) in 1/3 Ringer's solution at the one-cell stage (Mizoguchi et al., 2006). The embryos were then treated with inhibitors at 28.5 °C or with an equivalent amount of DMSO during 1- to 4-cell stage until fixation. The following inhibitors were used and all inhibitors were dissolved in DMSO: SB505124 (50 μM, Sigma-Aldrich), SB431542 (100 μM, Tocris Bioscience), SP600125 (10 μM, Cayman Chemical), EMD 420123 (50 μM, Merck Millipore), SB203580 (20 μM and 60 μM, Merck Millipore), NF-κB activation inhibitor (50 nM, Merck Millipore), ML141 (10 μM and 25 μM, Sigma-Aldrich), Y27632 (50 μM, Focus Biomolecules), LY294002 (10μm, Merck Millipore), and NSC23766 (150 μM and 300 μM, Merck Millipore). For nocodazole treatment, WT embryos with chorion were treated with nocodazole (66 μM, Sigma-Aldrich) (Brunet et al., 2013) from 3.8 hpf, and were fixed at 4.7 hpf.

mRNA injections

The pCS2+ vector carrying a cDNA fragment encoding *ndr1* (Rebagliati et al., 1998), *C-Syne2a* (Tsujikawa et al., 2007), *dn smad2* (Jia et al., 2008), *EGFP-smad2* (Dubrulle et al., 2015), *smad4a* (Hsu et al., 2011) , *mb-RFP* (Iioka et al., 2004), *mb-Venus* (Kinoshita et al., 2003), *H2B-mCherry* (Shiomi et al., 2017), or *nuclear lacZ* (*nlacZ*) was used in this study. Capped mRNA was synthesized using an SP6 mMESSAGE mMACHINE (Ambion). Embryos were injected with the following mRNAs: *C-syne2a* (500 pg), *dn smad2* (600 pg), *H2B-mCherry* (80 pg or 100 pg), *mb-Venus* (100 pg), *mb-RFP* (80 pg), *EGFP-smad2* (100 pg), *smad4a* (100 pg), and *nlacZ* mRNA (500 or 600 pg) at the one-cell stage. For the overexpression experiments into the YSL, *ndr1* or *nlacZ* mRNA (2880 pg each) with dextran-Alexa Fluor® 594 (Thermo Fisher Scientific) was injected into the YSL at 3 hpf.

Whole-mount *in situ* hybridization, immunohistochemistry, and FISH

Whole-mount *in situ* hybridization was performed as previously described (Westerfield, 1993), and riboprobes were prepared according to previously published methods.

Immunohistochemistry was performed as previously described (Hirose et al., 2013), with two overnight fixations, with the except of anti-α-tubulin antibody. For α-tubulin staining, embryos were fixed with 3.7 % formaldehyde and 0.25 % glutaraldehyde in a microtubule assembly buffer (80 mM KPIPES (pH 6.8), 5 mM EGTA, 1mM $MgCl_2$, 0.2% TritonX-100) (Topczewski and Solnica-Krezel, 1999). For double staining with anti-p-JNK and rhodamine-phalloidin, embryos were fixed with 3.7 % formaldehyde in PBS-Tween20

(PBSTw) for 2 h at room temperature; dehydration was omitted. Rhodamine-phalloidin (R415, Thermo Fisher Scientific) was used at a concentration of 1:100 for actin filament staining.

When FISH and immunohistochemistry were both required, immunohistochemistry was performed following FISH. Following hybridization with the *sox32* RNA probe, the embryos were sectioned and incubated in anti-digoxigenin-POD Fab fragments (Roche), which was diluted at 1:500 with 8 % sheep serum in PBSTw. After the tyramide signal amplification reaction, which was performed as previously described (Lauter et al., 2011), the sections were treated with the blocking buffer, and were incubated with primary antibody diluted in the same buffer. The following primary antibodies were used: anti-β-catenin rabbit polyclonal antibody at 1:300 (C-2206, Sigma-Aldrich); anti-γ-tubulin mouse monoclonal antibody at 1:500 (T6557, Sigma-Aldrich); anti-α-tubulin mouse monoclonal antibody at 1:5000 (T5168, Sigma-Aldrich); anti-phospho-Smad2 (Ser465/467) rabbit monoclonal antibody at 1:250 (04-953, Merck Millipore); anti Phospho-SAPK/JNK rabbit polyclonal antibody at 1:100 (#9251, Cell Signaling Technology). The following secondary antibodies were used: Alexa Fluor® 488 goat anti-rabbit IgG antibody at 1:500 (A11034, Thermo Fisher Scientific); Alexa Fluor® 594 goat anti-rabbit IgG antibody at 1:500 (A11037, Thermo Fisher Scientific); Alexa Fluor® 488 goat anti-mouse IgG antibody at 1:500 (A11029, Thermo Fisher Scientific). Nuclei were stained with 4',6-diamidino-2-phenylindole (DAPI) at a concentration of 1:1000.

Quantitative real-time PCR (qPCR) analyses

qPCR analyses were performed as previously described (Hirose et al., 2013). Total RNA was extracted from 20 - 40 embryos at 4.7 or 5.3 hpf using TRIzol (Thermo Fisher Scientific), and 500 ng DNase-treated RNA were reverse transcribed using olgo-(dT) primers and Reverse transcriptase XL (TAKARA). qPCR for four genes (*ndr1*, *ndr2*, *ta*, and *sox32*) was performed in triplicates or tetraplicates with the Thermal Cycler Dice Real-Time system II and SYBR Premix Ex Taq II (TAKARA), according to the manufacturer's instructions. Zebrafish *ribosomal protein L13a* (*rpl13a*) was used as a reference gene. The qPCR primers are listed in Table S1. *p* values were calculated using the Student's *t*-test.

Imaging analysis

Images were acquired using an Olympus FV1000-D confocal microscope system. Confocal live imaging was performed as previously described (Mizoguchi et al., 2008). Confocal time-lapse imaging was performed on the same confocal microscope using a 60× water immersion lens. We recorded Z-stacks (0.62 μm steps) at 5 min intervals, and analyzed the images using the ImageJ software (NIH). The p-JNK intensities at the cell membranes of LMCs were analyzed using ImageJ by measuring the mean gray value of a three pixel width line drawn along the cell membrane on the boundary between the YSL and LMCs, between cells located at the animal-pole side and LMCs, between EVL and LMCs, or between MMCs and LMCs (Morrissey et al., 2016). Cytoplasmic background signals were subtracted from each of the mean gray values. Average values and standard deviations were

determined from 10 LMCs of DMSO- or SB505124-treated embryos. To measure cytoplasmic area occupied by MTs, one fluorescent image of MTs was converted to grayscale, and the area of MTs and cytoplasm were determined by threshold analysis and freehand selection in the ImageJ software, respectively (Wadsworth and McGrail, 1990, Craig et al., 2010).

Statistical analyses

Data were expressed as averages from repeated experiments with standard deviation. Statistical significance was determined by using the Student's *t*-test. *p* values of ≤ 0.05 was considered to be statistically significant.

ACKNOWLEDGEMENTS

We thank Dr. Anming Meng for pCS2-*dn smad2*; Dr. Noriyuki Kinoshita for pCS2-*mb-RFP* and pCS2-*mb-Venus*; Dr. Hiroshi Kimura for pCS2-*H2B-mCherry*; Institute for Amphibian Biology in Hiroshima University for cryostat sectioning and qPCR; the members of Kikuchi and Atsushi Suzuki laboratories in Hiroshima University for helpful discussion and critical comments. This work was supported by the Hiroshima University Grant-in-Aid for Exploratory Research (The researcher support of young Scientists) to S.H.

COMPETING INTERESTs

The authors have no competing interests to declare.

AUTHOR CONTRIBUTIONS

SH, SA, and YK designed research. SH and SA performed research. SH and YK wrote the paper.

REFERENCES

ALEXANDER, J., ROTHENBERG, M., HENRY, G. L. & STAINIER, D. Y. 1999. casanova plays an early and essential role in endoderm formation in zebrafish. *Dev Biol,* 215**,** 343-57.

BENNETT, B. L., SASAKI, D. T., MURRAY, B. W., O'LEARY, E. C., SAKATA, S. T., XU, W., LEISTEN, J. C., MOTIWALA, A., PIERCE, S., SATOH, Y., BHAGWAT, S. S., MANNING, A. M. & ANDERSON, D. W. 2001. SP600125, an anthrapyrazolone inhibitor of Jun N-terminal kinase. *Proc Natl Acad Sci U S A,* 98**,** 13681-6.

BONE, C. R. & STARR, D. A. 2016. Nuclear migration events throughout development. *J Cell Sci,* 129**,** 1951-61.

BRUNET, T., BOUCLET, A., AHMADI, P., MITROSSILIS, D., DRIQUEZ, B., BRUNET, A. C., HENRY, L., SERMAN, F., B ALLE, G., M NAGER, C., DUMAS-BOUCHIAT, F., GIVORD, D., YANICOSTAS, C., LE-ROY, D., DEMPSEY, N. M., PLESSIS, A. & FARGE, E. 2013. Evolutionary conservation of early mesoderm specification by mechanotransduction in Bilateria. *Nat Commun,* 4**,** 2821.

CALLAHAN, J. F., BURGESS, J. L., FORNWALD, J. A., GASTER, L. M., HARLING, J. D., HARRINGTON, F. P., HEER, J., KWON, C., LEHR, R., MATHUR, A., OLSON, B. A., WEINSTOCK, J. & LAPING, N. J. 2002. Identification of novel inhibitors of the transforming growth factor beta1 (TGF-beta1) type 1 receptor (ALK5). *J Med Chem,* 45**,** 999-1001.

CRAIG, S. E., THUMMEL, R., AHMED, H., VASTA, G. R., HYDE, D. R. & HITCHCOCK, P. F. 2010. The zebrafish galectin Drgal1-l2 is expressed by proliferating Müller glia and photoreceptor progenitors and regulates the regeneration of rod photoreceptors. *Invest Ophthalmol Vis Sci,* 51**,** 3244-52.

CUENDA, A., ROUSE, J., DOZA, Y. N., MEIER, R., COHEN, P., GALLAGHER, T. F., YOUNG, P. R. & LEE, J. C. 1995. SB 203580 is a specific inhibitor of a MAP kinase homologue which is stimulated by cellular stresses and interleukin-1. *FEBS Lett,* 364**,** 229-33.

DACOSTA BYFIELD, S., MAJOR, C., LAPING, N. J. & ROBERTS, A. B. 2004. SB-505124 is a selective inhibitor of transforming growth factor-beta type I receptors ALK4, ALK5, and ALK7. *Mol Pharmacol,* 65**,** 744-52.

DEL BENE, F., WEHMAN, A. M., LINK, B. A. & BAIER, H. 2008. Regulation of neurogenesis by interkinetic nuclear migration through an apical-basal notch gradient. *Cell,* 134**,** 1055-65.

DERYNCK, R. & ZHANG, Y. E. 2003. Smad-dependent and Smad-independent pathways in TGF-beta family signalling. *Nature,* 425**,** 577-84.

DI GUGLIELMO, G. M., LE ROY, C., GOODFELLOW, A. F. & WRANA, J. L. 2003. Distinct endocytic pathways regulate TGF-beta receptor signalling and turnover. *Nat Cell Biol,* 5**,** 410-21.

DICKMEIS, T., MOURRAIN, P., SAINT-ETIENNE, L., FISCHER, N., AANSTAD, P., CLARK, M., STR HLE, U. & ROSA, F. 2001. A crucial component of the endoderm

formation pathway, CASANOVA, is encoded by a novel sox-related gene. *Genes Dev,* 15**,** 1487-92.

DUBRULLE, J., JORDAN, B. M., AKHMETOVA, L., FARRELL, J. A., KIM, S. H., SOLNICA-KREZEL, L. & SCHIER, A. F. 2015. Response to Nodal morphogen gradient is determined by the kinetics of target gene induction. *Elife,* 4.

DUPIN, I. & ETIENNE-MANNEVILLE, S. 2011. Nuclear positioning: mechanisms and functions. *Int J Biochem Cell Biol,* 43**,** 1698-707.

FELDMAN, B., GATES, M. A., EGAN, E. S., DOUGAN, S. T., RENNEBECK, G., SIROTKIN, H. I., SCHIER, A. F. & TALBOT, W. S. 1998. Zebrafish organizer development and germ-layer formation require nodal-related signals. *Nature,* 395**,** 181-5.

FUKUDA, K. & KIKUCHI, Y. 2005. Endoderm development in vertebrates: fate mapping, induction and regional specification. *Dev Growth Differ,* 47**,** 343-55.

GAO, Y., DICKERSON, J. B., GUO, F., ZHENG, J. & ZHENG, Y. 2004. Rational design and characterization of a Rac GTPase-specific small molecule inhibitor. *Proc Natl Acad Sci U S A,* 101**,** 7618-23.

GRIMM, O. H. & GURDON, J. B. 2002. Nuclear exclusion of Smad2 is a mechanism leading to loss of competence. *Nat Cell Biol,* 4**,** 519-22.

GRITSMAN, K., ZHANG, J., CHENG, S., HECKSCHER, E., TALBOT, W. S. & SCHIER, A. F. 1999. The EGF-CFC protein one-eyed pinhead is essential for nodal signaling. *Cell,* 97**,** 121-32.

GUNDERSEN, G. G. & WORMAN, H. J. 2013. Nuclear positioning. *Cell,* 152**,** 1376-89.

HAN, Z., BOYLE, D. L., CHANG, L., BENNETT, B., KARIN, M., YANG, L., MANNING, A. M. & FIRESTEIN, G. S. 2001. c-Jun N-terminal kinase is required for metalloproteinase expression and joint destruction in inflammatory arthritis. *J Clin Invest,* 108**,** 73-81.

HARVEY, S. A. & SMITH, J. C. 2009. Visualisation and quantification of morphogen gradient formation in the zebrafish. *PLoS Biol,* 7**,** e1000101.

HAYES, S., CHAWLA, A. & CORVERA, S. 2002. TGF beta receptor internalization into EEA1-enriched early endosomes: role in signaling to Smad2. *J Cell Biol,* 158**,** 1239-49.

HIROSE, K., SHIMODA, N. & KIKUCHI, Y. 2013. Transient reduction of 5-methylcytosine and 5-hydroxymethylcytosine is associated with active DNA demethylation during regeneration of zebrafish fin. *Epigenetics,* 8**,** 899-906.

HSU, R. J., LIN, C. C., SU, Y. F. & TSAI, H. J. 2011. dickkopf-3-related gene regulates the expression of zebrafish myf5 gene through phosphorylated p38a-dependent Smad4 activity. *J Biol Chem,* 286**,** 6855-64.

HUSE, M. 2012. Microtubule-organizing center polarity and the immunological synapse: protein kinase C and beyond. *Front Immunol,* 3**,** 235.

IIOKA, H., UENO, N. & KINOSHITA, N. 2004. Essential role of MARCKS in cortical actin dynamics during gastrulation movements. *J Cell Biol,* 164**,** 169-74.

INMAN, G. J., NICOL S, F. J., CALLAHAN, J. F., HARLING, J. D., GASTER, L. M., REITH, A. D., LAPING, N. J. & HILL, C. S. 2002. SB-431542 is a potent and specific inhibitor of transforming growth factor-beta superfamily type I activin receptor-like kinase (ALK) receptors ALK4, ALK5, and ALK7. *Mol Pharmacol,* 62**,** 65-74.

JIA, S., REN, Z., LI, X., ZHENG, Y. & MENG, A. 2008. smad2 and smad3 are required for mesendoderm induction by transforming growth factor-beta/nodal signals in zebrafish. *J Biol Chem,* 283**,** 2418-26.

KENYON, E. J., CAMPOS, I., BULL, J. C., WILLIAMS, P. H., STEMPLE, D. L. & CLARK, M. D. 2015. Zebrafish Rab5 proteins and a role for Rab5ab in nodal signalling. *Dev Biol,* 397**,** 212-24.

KIKUCHI, Y., AGATHON, A., ALEXANDER, J., THISSE, C., WALDRON, S., YELON, D., THISSE, B. & STAINIER, D. Y. 2001. casanova encodes a novel Sox-related protein necessary and sufficient for early endoderm formation in zebrafish. *Genes Dev,* 15**,** 1493-505.

KIMMEL, C. B., BALLARD, W. W., KIMMEL, S. R., ULLMANN, B. & SCHILLING, T. F. 1995. Stages of embryonic development of the zebrafish. *Dev Dyn,* 203**,** 253-310.

KINOSHITA, N., IIOKA, H., MIYAKOSHI, A. & UENO, N. 2003. PKC delta is essential for Dishevelled function in a noncanonical Wnt pathway that regulates Xenopus convergent extension movements. *Genes Dev,* 17**,** 1663-76.

LAPING, N. J., GRYGIELKO, E., MATHUR, A., BUTTER, S., BOMBERGER, J., TWEED, C., MARTIN, W., FORNWALD, J., LEHR, R., HARLING, J., GASTER, L., CALLAHAN, J. F. & OLSON, B. A. 2002. Inhibition of transforming growth factor (TGF)-beta1-induced extracellular matrix with a novel inhibitor of the TGF-beta type I receptor kinase activity: SB-431542. *Mol Pharmacol,* 62**,** 58-64.

LAUTER, G., SOLL, I. & HAUPTMANN, G. 2011. Multicolor fluorescent in situ hybridization to define abutting and overlapping gene expression in the embryonic zebrafish brain. *Neural Dev,* 6**,** 10.

LI, C., GE, B., NICOTRA, M., STERN, J. N., KOPCOW, H. D., CHEN, X. & STROMINGER, J. L. 2008. JNK MAP kinase activation is required for MTOC and granule polarization in NKG2D-mediated NK cell cytotoxicity. *Proc Natl Acad Sci U S A,* 105**,** 3017-22.

LIU, X., XIONG, C., JIA, S., ZHANG, Y., CHEN, Y. G., WANG, Q. & MENG, A. 2013. Araf kinase antagonizes Nodal-Smad2 activity in mesendoderm development by directly phosphorylating the Smad2 linker region. *Nat Commun,* 4**,** 1728.

MASSAGUE, J. 2003. Integration of Smad and MAPK pathways: a link and a linker revisited. *Genes Dev,* 17**,** 2993-7.

MIZOGUCHI, T., IZAWA, T., KUROIWA, A. & KIKUCHI, Y. 2006. Fgf signaling negatively regulates Nodal-dependent endoderm induction in zebrafish. *Dev Biol,* 300**,** 612-22.

MIZOGUCHI, T., VERKADE, H., HEATH, J. K., KUROIWA, A. & KIKUCHI, Y. 2008. Sdf1/Cxcr4 signaling controls the dorsal migration of endodermal cells during zebrafish gastrulation. *Development,* 135**,** 2521-9.

MORI, S., MATSUZAKI, K., YOSHIDA, K., FURUKAWA, F., TAHASHI, Y., YAMAGATA, H., SEKIMOTO, G., SEKI, T., MATSUI, H., NISHIZAWA, M., FUJISAWA, J. & OKAZAKI, K. 2004. TGF-beta and HGF transmit the signals through JNK-dependent Smad2/3 phosphorylation at the linker regions. *Oncogene,* 23**,** 7416-29.

MORRISSEY, M. A., JAYADEV, R., MILEY, G. R., BLEBEA, C. A., CHI, Q., IHARA, S. & SHERWOOD, D. R. 2016. SPARC Promotes Cell Invasion In Vivo by Decreasing Type IV Collagen Levels in the Basement Membrane. *PLoS Genet,* 12**,** e1005905.

MOUSTAKAS, A. & HELDIN, C. H. 2005. Non-Smad TGF-beta signals. *J Cell Sci,* 118**,** 3573-84.

MU, Y., GUDEY, S. K. & LANDSTR M, M. 2012. Non-Smad signaling pathways. *Cell Tissue Res,* 347**,** 11-20.

NOMURA, M. & LI, E. 1998. Smad2 role in mesoderm formation, left-right patterning and craniofacial development. *Nature,* 393**,** 786-90.

OBER, E. A., FIELD, H. A. & STAINIER, D. Y. 2003. From endoderm formation to liver and pancreas development in zebrafish. *Mech Dev,* 120**,** 5-18.

PENHEITER, S. G., MITCHELL, H., GARAMSZEGI, N., EDENS, M., DOR , J. J. & LEOF, E. B. 2002. Internalization-dependent and -independent requirements for transforming growth factor beta receptor signaling via the Smad pathway. *Mol Cell Biol,* 22**,** 4750-9.

REBAGLIATI, M. R., TOYAMA, R., FRICKE, C., HAFFTER, P. & DAWID, I. B. 1998. Zebrafish nodal-related genes are implicated in axial patterning and establishing left-right asymmetry. *Dev Biol,* 199**,** 261-72.

RODAWAY, A., TAKEDA, H., KOSHIDA, S., BROADBENT, J., PRICE, B., SMITH, J. C., PATIENT, R. & HOLDER, N. 1999. Induction of the mesendoderm in the zebrafish germ ring by yolk cell-derived TGF-beta family signals and discrimination of mesoderm and endoderm by FGF. *Development,* 126**,** 3067-78.

SCHIER, A. F. 2009. Nodal morphogens. *Cold Spring Harb Perspect Biol,* 1**,** a003459.

SHIOMI, T., MUTO, A., HOZUMI, S., KIMURA, H. & KIKUCHI, Y. 2017. Histone H3 Lysine 27 Trimethylation Leads to Loss of Mesendodermal Competence During Gastrulation in Zebrafish Ectodermal Cells. *Zoolog Sci,* 34**,** 64-71.

STARR, D. A. 2009. A nuclear-envelope bridge positions nuclei and moves chromosomes. *J Cell Sci,* 122**,** 577-86.

TOBE, M., ISOBE, Y., TOMIZAWA, H., NAGASAKI, T., TAKAHASHI, H. & HAYASHI, H. 2003. A novel structural class of potent inhibitors of NF-kappa B activation: structure-activity relationships and biological effects of 6-aminoquinazoline derivatives. *Bioorg Med Chem,* 11**,** 3869-78.

TOPCZEWSKI, J. & SOLNICA-KREZEL, L. 1999. Cytoskeletal dynamics of the zebrafish embryo. *Methods Cell Biol,* 59**,** 205-26.

TSUJIKAWA, M., OMORI, Y., BIYANWILA, J. & MALICKI, J. 2007. Mechanism of positioning the cell nucleus in vertebrate photoreceptors. *Proc Natl Acad Sci U S A,* 104**,** 14819-24.

VLAHOS, C. J., MATTER, W. F., HUI, K. Y. & BROWN, R. F. 1994. A specific inhibitor of phosphatidylinositol 3-kinase, 2-(4-morpholinyl)-8-phenyl-4H-1-benzopyran-4-one (LY294002). *J Biol Chem,* 269**,** 5241-8.

WADSWORTH, P. & MCGRAIL, M. 1990. Interphase microtubule dynamics are cell type-specific. *J Cell Sci,* 95 (Pt 1)**,** 23-32.

WEINSTEIN, M., YANG, X., LI, C., XU, X., GOTAY, J. & DENG, C. X. 1998. Failure of egg cylinder elongation and mesoderm induction in mouse embryos lacking the tumor suppressor smad2. *Proc Natl Acad Sci U S A,* 95**,** 9378-83.

WESTERFIELD, M. 1993. *The zebrafish book : a guide for the laboratory use of zebrafish (Brachydanio rerio),* Eugene, OR, M. Westerfield.

WRIGHTON, K. H., LIN, X. & FENG, X. H. 2009. Phospho-control of TGF-beta superfamily signaling. *Cell Res,* 19**,** 8-20.

ZORN, A. M. & WELLS, J. M. 2009. Vertebrate endoderm development and organ formation. *Annu Rev Cell Dev Biol,* 25**,** 221-51.

Figures

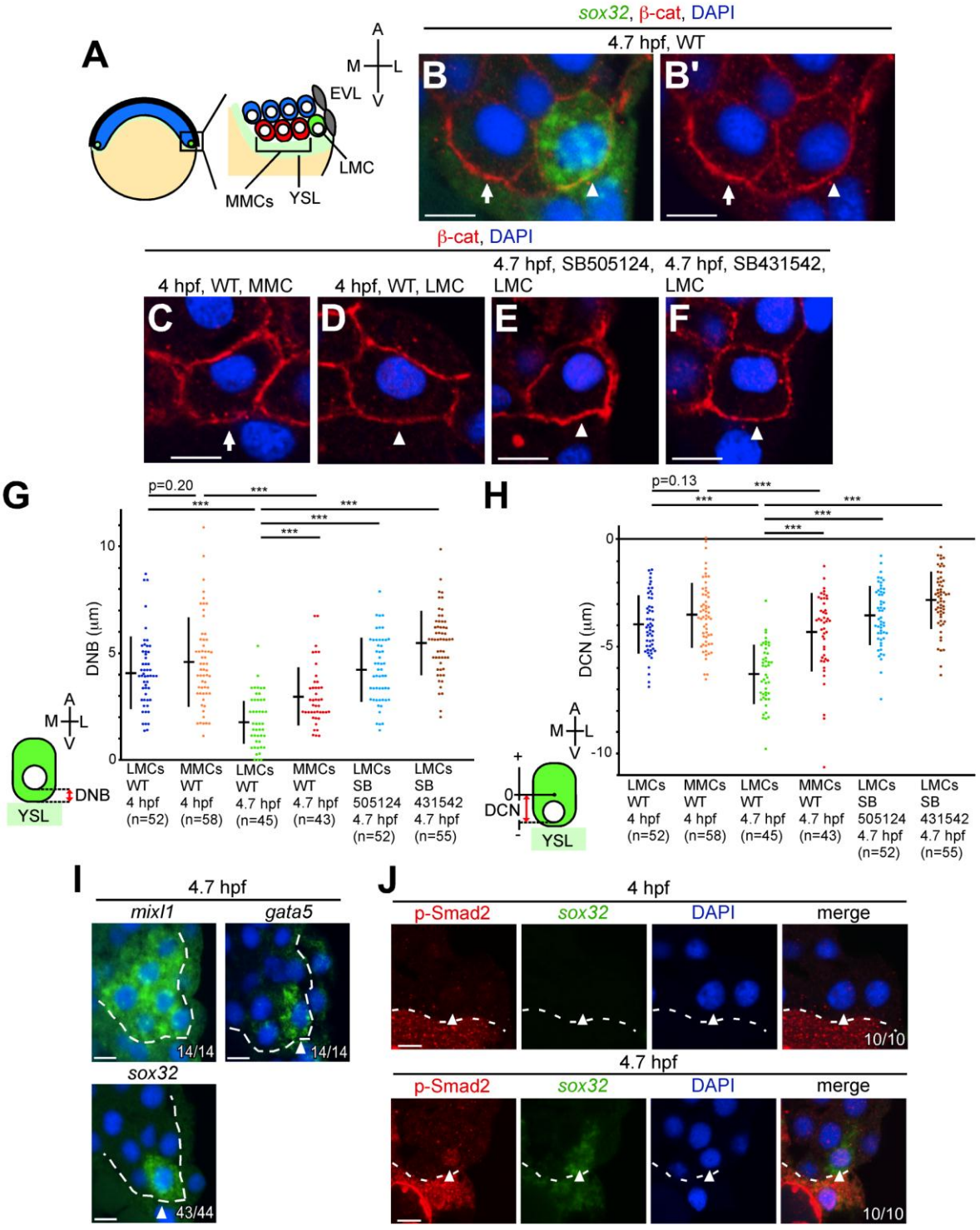

Figure 1. Nuclear movement toward the YSL in LMCs occurs at 4.7 hpf

(A) Illustration of zebrafish blastula embryos and location of marginal cells. LMCs: the most laterally located marginal cells (green); MMCs: medial marginal cells (red). A: animal; V: vegetal; M: medial; L:lateral. (B-F) Cross sections of wild-type (WT) and TGF-β type I receptor inhibitor (SB505124 or SB431542)-treated embryos; the cell membrane and the nucleus were visualized by β-Catenin (β-cat) staining (red) and 4,6-diamidino-2-phenylindole dihydrochloride (DAPI, blue) staining, respectively. The endoderm marker *sox32* (green) was detected by fluorescent *in situ* hybridization (FISH) (B). White arrows and arrowheads indicate MMCs and LMCs, respectively. Scale bars: 10 μm. (G) Minimum distance between the most vegetal position of the nucleus and the blastoderm/YSL boundary (DNBs) in WT and TGF-β receptor inhibitor-treated embryos. ***$p < 0.001$. (H) Minimum distance between the center of the cell and the most vegetal position of the nucleus (DCNs) relative to the animal-vegetal axis in WT and TGF-β receptor inhibitor-treated embryos. In the DCN, the center of cell is defined as zero; the animal and vegetal sides relative to the center of cell are set as plus and minus along the animal and vegetal axis, respectively. ***$p < 0.001$. n = number of nuclei examined (G, H). (I) Cross sections of WT embryos; *mixl1*, *gata5*, and *sox32* were visualized via FISH at 4.7 hpf. The number of embryos examined is shown at the lower right corner of the panel. DAPI was used for visualization of nucleus. White arrowheads indicate LMCs. White dotted lines indicate the boundary between the blastoderm and the YSL or EVL. Scale bars:

10 μm. (J) Cross sections of WT embryos; p-Smad2 and *sox32* were visualized via immunohistochemical staining and FISH, respectively. The number of embryos examined is shown at the lower right corner of the merge panel. DAPI was used for visualization of nucleus. White arrowheads indicate the nucleus in LMC. White dotted lines indicate the boundary between the blastoderm and the YSL. Scale bars: 10 μm.

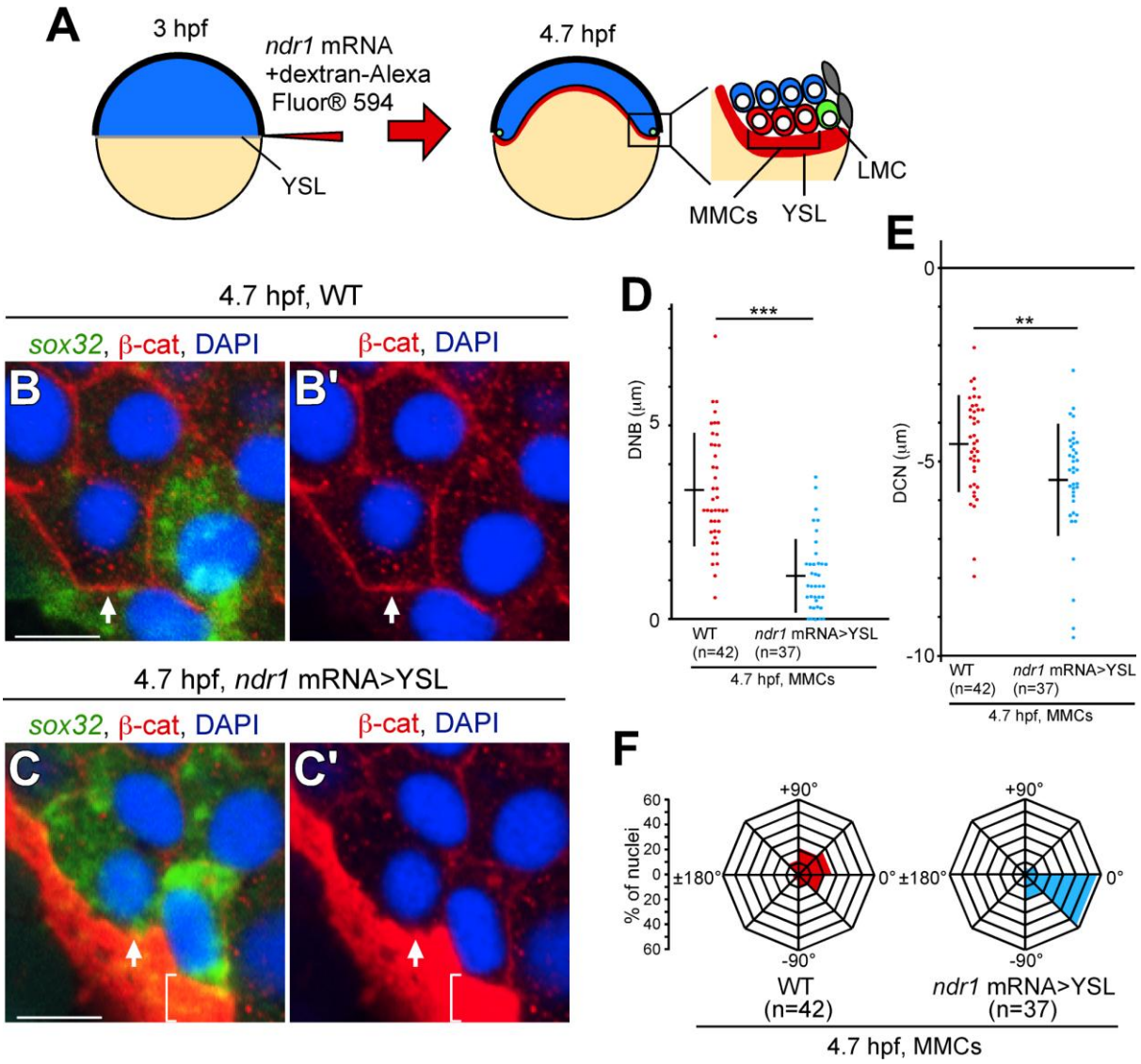

Figure 2. Overexpression of *ndr1* mRNA in YSL leads to nuclear movement in MMCs toward the YSL

(A) Illustration of the experimental design for *ndr1* mRNA overexpression into YSL (*ndr1* mRNA>YSL). (B-C') Cross sections of WT and *ndr1* mRNA>YSL embryos; the cell membrane, nucleus, and *sox32* mRNA were visualized by β-cat staining, DAPI staining, and FISH, respectively at 4.7 hpf. White arrowheads indicate the MMCs. White brackets indicate the fluorescence of dextran-Alexa Fluor® 594 in the YSL. Both nuclear movement and *sox32* expression in MMCs were induced by *ndr1* mRNA>YSL at 4.7 hpf. Scale bars:

10 μm. (D, E) DNBs and DCNs in MMCs were measured in WT and *ndr1* mRNA>YSL embryos. ***$p < 0.001$. (F) Angles between the center of the cell and the nucleus relative to the medial-lateral axis were measured in WT and *ndr1* mRNA>YSL embryos as shown in Figure S1. n = number of nuclei examined (D-F).

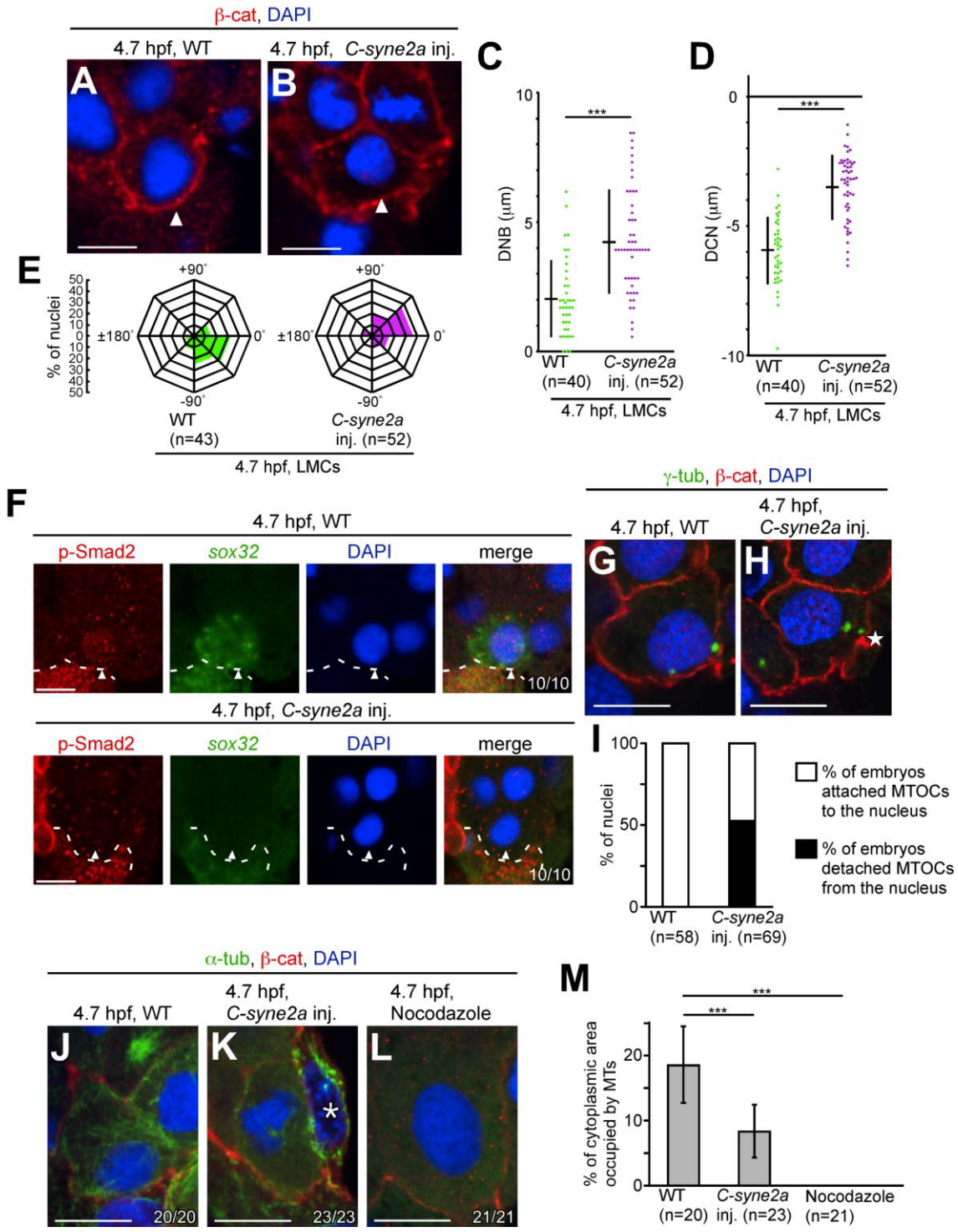

Figure 3. *C-syne2a* overexpression prevents nuclear movement and p-Smad2 nuclear translocation in LMCs, possibly through regulation of MTOC positioning and MT formation

(A-B) Nuclear positioning in LMCs in WT and *C-syne2a*-overexpressing embryos at 4.7 hpf. Cross sections of WT and *C-syne2a*-overexpressing embryos; cell membrane and nucleus were visualized by β-cat and DAPI staining, respectively. Scale bars: 10 μm. (C, D) DNBs and DCNs in LMCs were measured in WT and *C-syne2a*-overexpressing embryos at 4.7 hpf. n = number of nuclei examined. ***$p < 0.001$. (E) Angles between the center of the cell and the nucleus in LMCs relative to the medial-lateral axis were measured as shown in Figure S1. n = number of nuclei examined. (F) Cross sections of WT embryos; p-Smad2 and *sox32* were visualized by immunohistochemical staining and FISH, respectively. The number of nuclei examined is shown at the lower right corner of the merge panel. DAPI was used for visualization of nuclei. White arrowheads indicate the nuclei in LMCs. White dotted lines indicate the boundary between the blastoderm and the YSL. Scale bars: 10 μm. (G, H) Cross sections of WT and *C-syne2a*-overexpressing embryos; cell membrane and MTOCs were visualized by β-cat and γ-tubulin (γ-tub) staining, respectively at 4.7 hpf. DAPI was used for visualization of nuclei. Scale bars: 10 μm. The white star indicates MTOC that has detached from the nucleus in *C-syne2a*-overexpressing embryos (H). (I) Percentage of embryos with attached or detached MTOCs in WT or *C-syne2a*-overexpressing embryos at 4.7 hpf. n = number of nuclei examined. (J-L) Cross sections of WT, *C-syne2a*-overexpressing, and nocodazole treated embryos; cell membrane, MTs, and nuclei were visualized by β-cat, α-tubulin (α-tub), and DAPI staining, respectively at 4.7 hpf. The number of embryos examined is shown at the lower right corner of each panel. An asterisk indicates the EVL cell. Scale bars:

10 µm. (M) Percentage of cytoplasmic area occupied by MTs in LMCs of WT, *C-syne2a*-overexpressing, and nocodazole-treated embryos. n = number of embryos examined. ***$p < 0.001$.

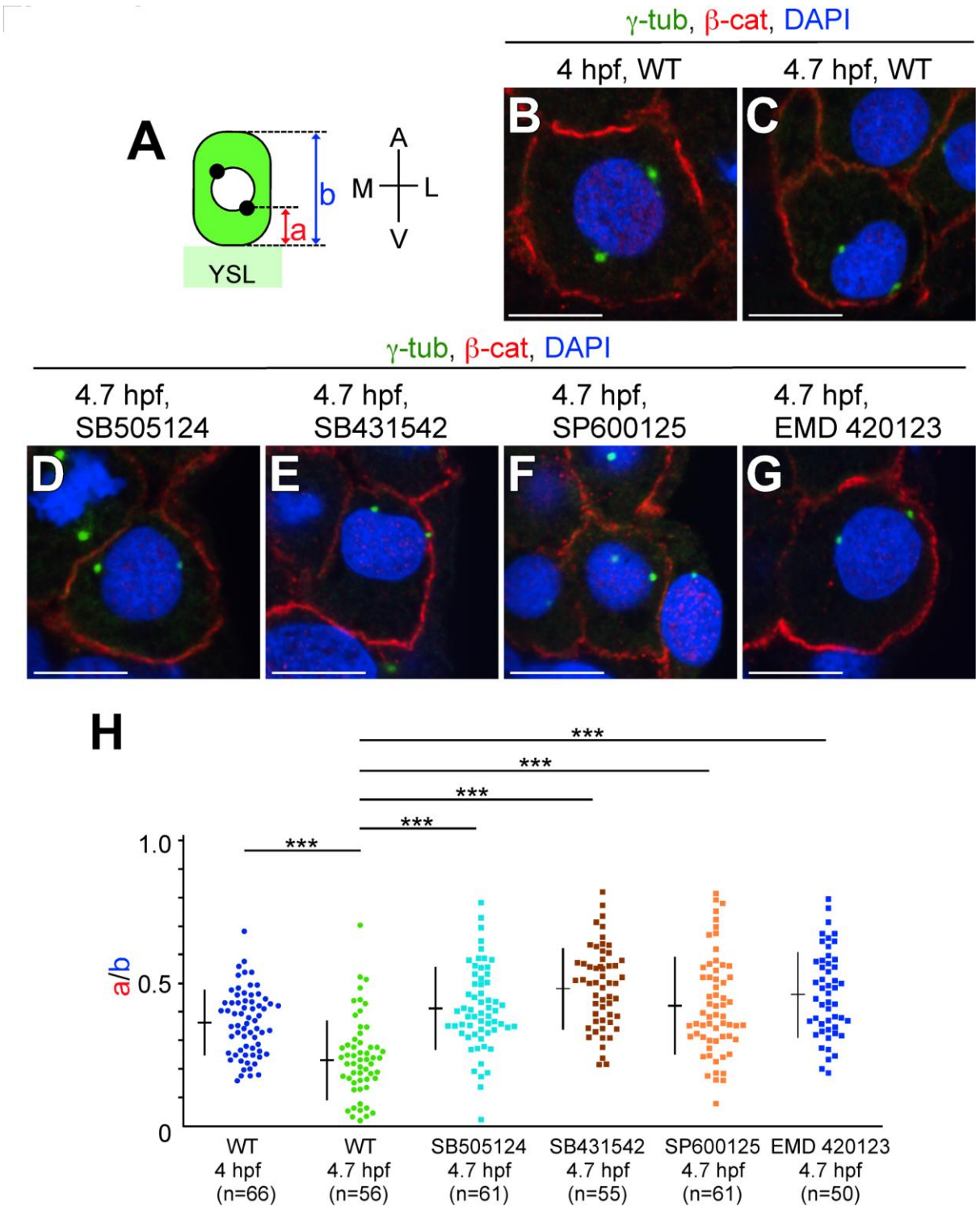

Figure 4. MTOC reorientation in LMCs is regulated by Nodal/JNK signaling

(A) Illustration of MTOC positioning (black dots) in LMCs. a, the minimum distance between the most vegetal position of MTOCs and the blastoderm/YSL boundary; b, length of the LMC. (B-G) Cross sections of WT, SB505124-, SB431542-, SP600125-, and EMD

420123-treated embryos; MTOCs, cell membrane, and nuclei were visualized by γ-tub, β-cat, and DAPI staining, respectively at 4.0 and/or 4.7 hpf. Scale bars: 10 μm. (H) a/b ratio in WT, SB505124-, SB431542-, SP600125-, or EMD 420123-treated embryos at 4.0 or 4.7 hpf. n = the number of nuclei examined. ***$p < 0.001$.

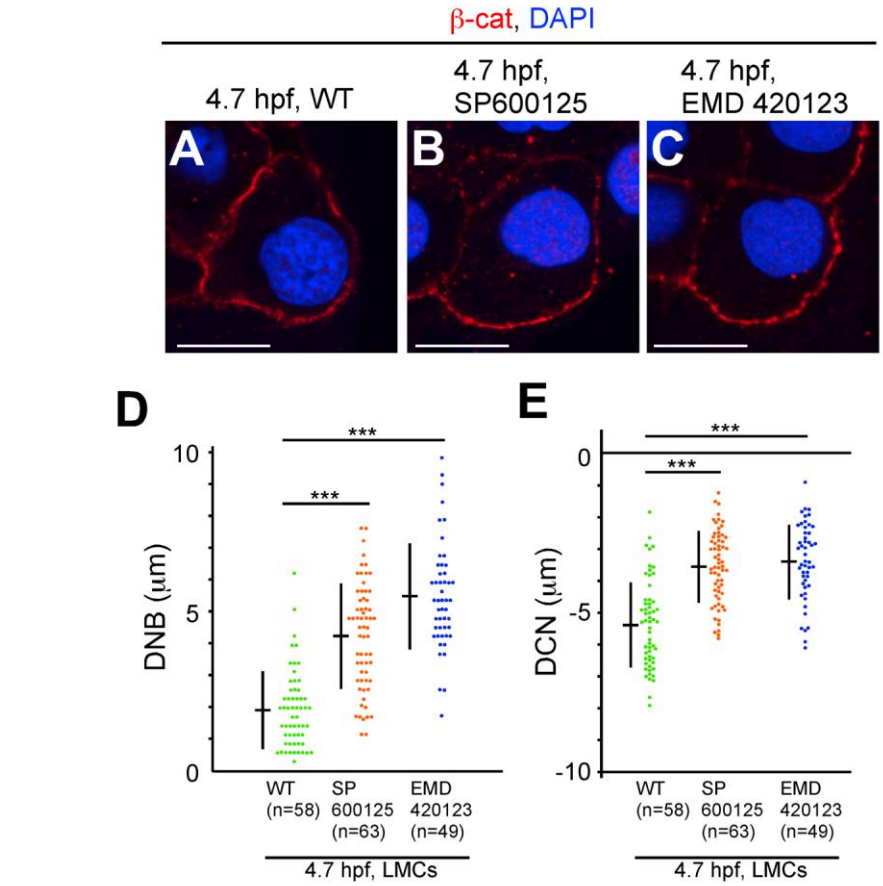

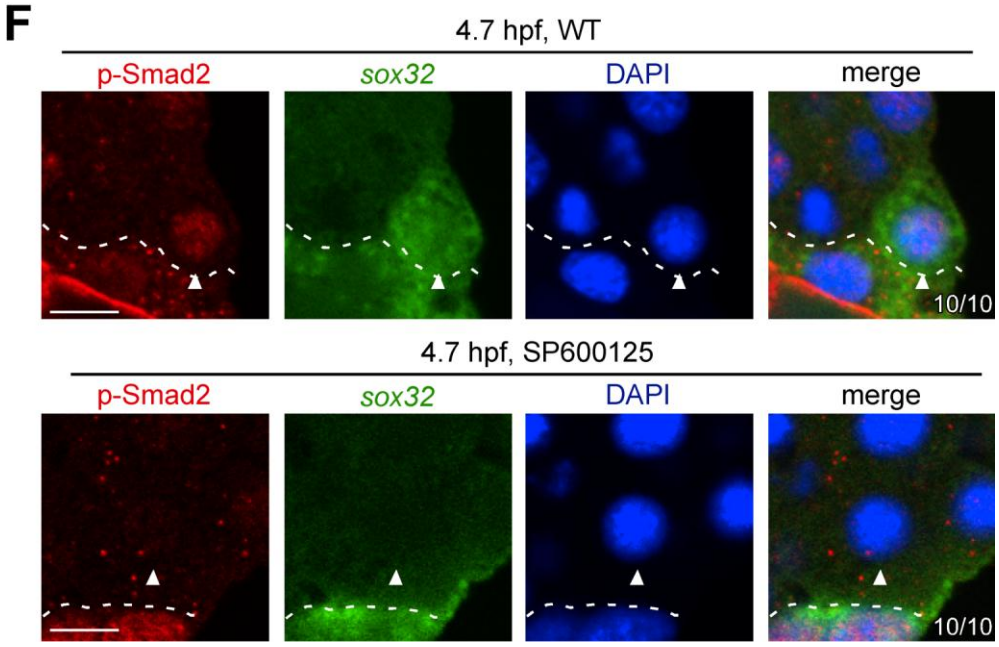

Figure 5. Inhibition of JNK signaling suppresses nuclear movement and p-Smad2 nuclear translocation in LMCs

(A-C) Cross sections of WT, SP600125-, and EMD 420123-treated embryos; cell membrane and nuclei were visualized by β-cat and DAPI staining, respectively at 4.7 hpf. Scale bars: 10 μm. (D, E) DNBs and DCNs in LMCs were measured in WT, SP600125- or EMD 420123-treated embryos. ***$p < 0.001$. (F) Cross sections of WT and SP600125-treated embryos; p-Smad2 and *sox32* were visualized by immunohistochemical staining and FISH, respectively. The number of embryos examined is shown at the lower right corner of the merge panel. DAPI was used for visualization of nuclei. White arrowheads indicate the nuclei in LMCs. White dotted lines indicate the boundary between the blastoderm and the YSL. Scale bars: 10 μm.

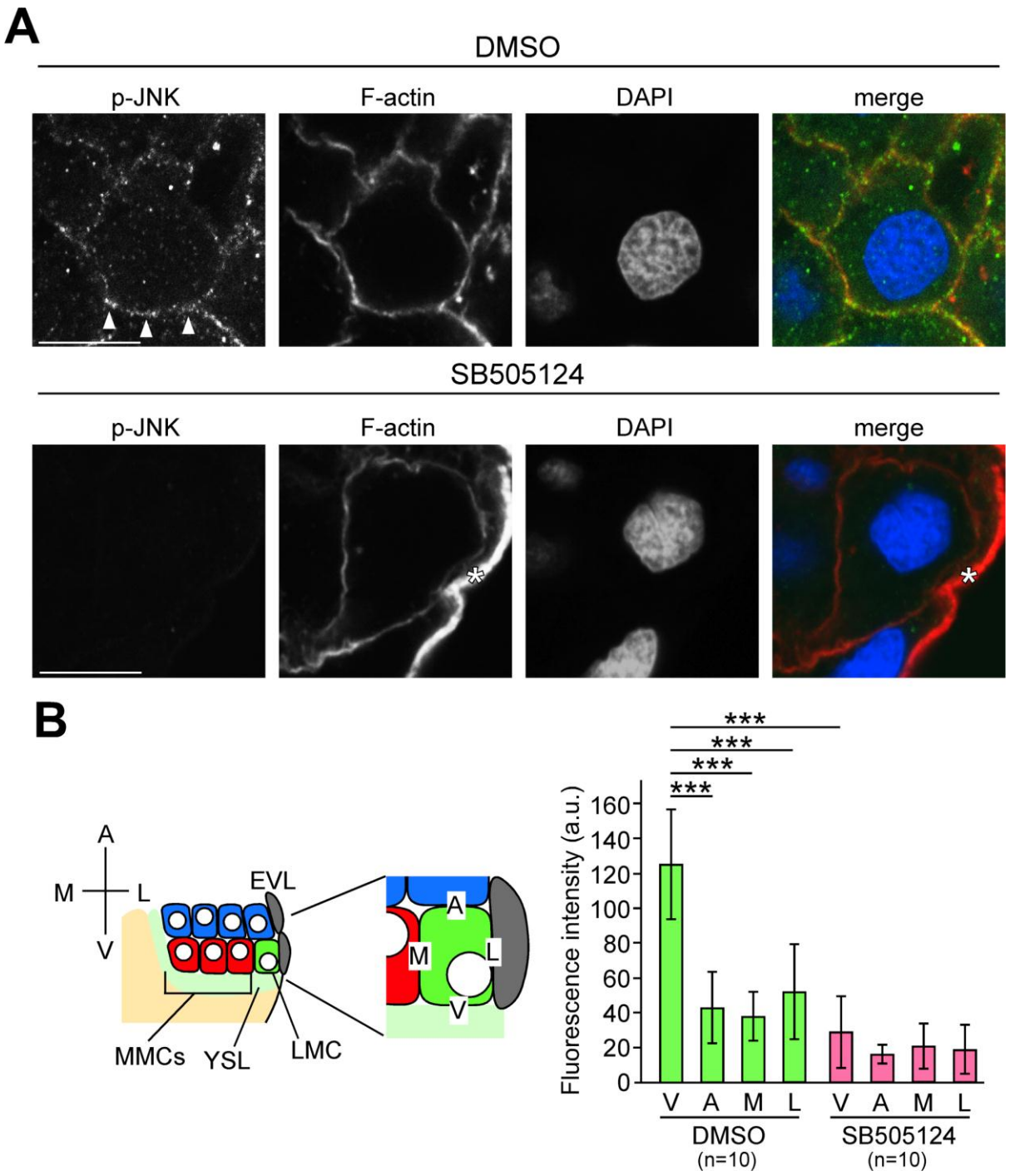

Figure 6. JNK is activated by Nodal from the YSL

(A) Cross sections of DMSO- and SB505124-treated embryos; p-JNK and filamentous actin were visualized by immunohistochemical staining and phalloidin, respectively at 4.7 hpf. Fluorescent signals are displayed as gray scale images. DAPI was used for visualization of nuclei. White arrowheads indicate p-JNK fluorescence on the boundary between the YSL

and LMCs. Asterisks indicate the cell membrane of EVL cells. Scale bars: 10 μm. (B) Fluorescent intensities were measured along the cell membrane on the boundaries between: the YSL and LMCs (V), cells located animal-pole side and LMCs (A), EVL and LMCs (L), or MMCs and LMCs (M). Error bars represent standard deviations of 10 measurements. n = number of nuclei examined. ***$p < 0.001$.

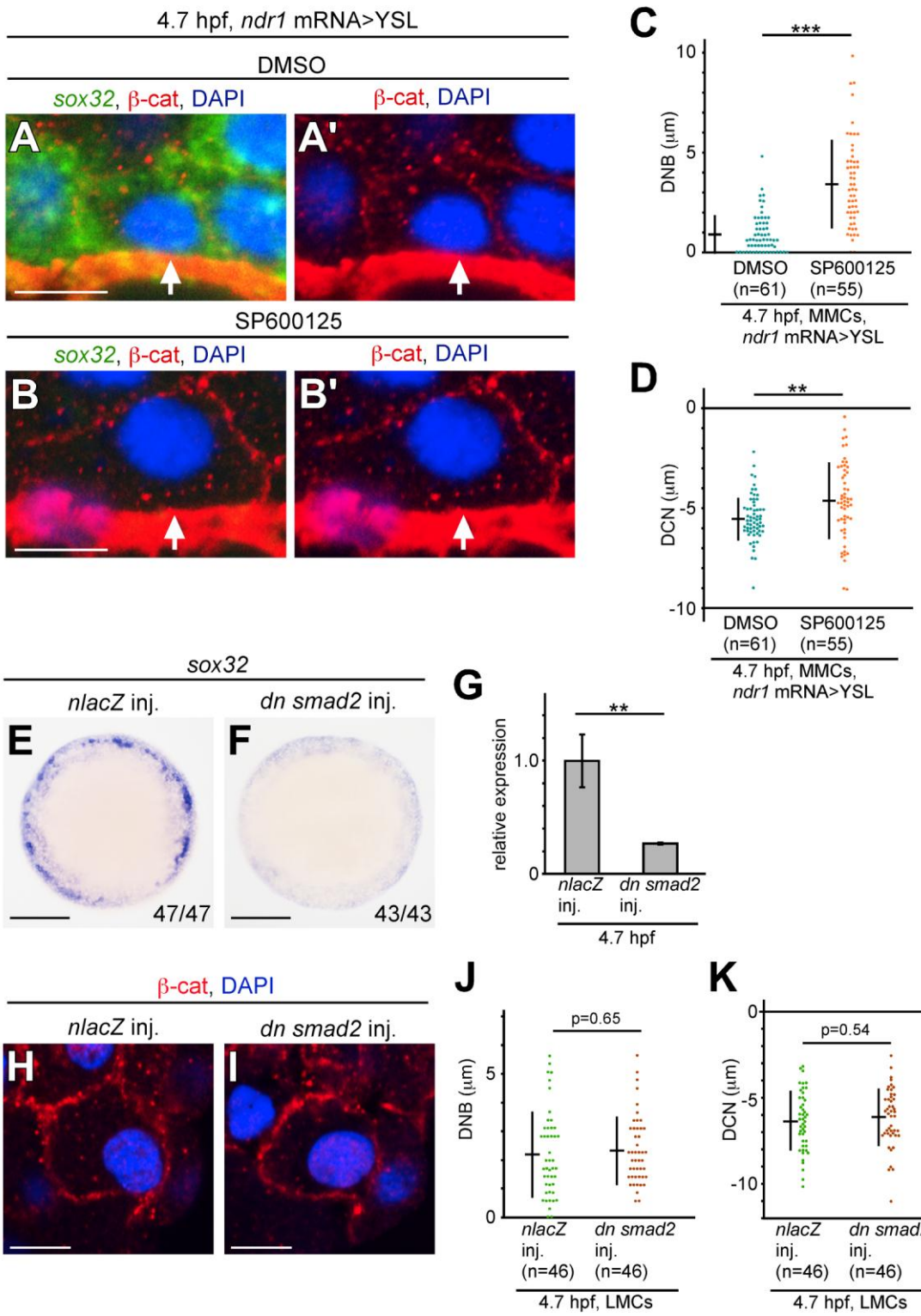

Figure 7. Nuclear movement is regulated by non-Smad JNK signaling independent of Smad signaling

(A-B') Cross sections of *ndr1* mRNA>YSL embryos treated with DMSO (A, A') and SP600125 (B, B'); the cell membrane, nucleus, and *sox32* mRNA were visualized by β-cat staining, DAPI staining, and FISH, respectively at 4.7 hpf. White arrows indicate the nuclei in MMCs. Scale bars: 10 μm. (C, D) Mean DNB and DCN values in MMCs of *ndr1* mRNA>YSL embryos treated with SP600125 or DMSO at 4.7 hpf. n = number of nuclei examined. ***$p < 0.001$, **$p < 0.05$. (E, F) WISH of *sox32* expression in *nuclear lacZ* (*nlacZ*) or *dn smad2* mRNA overexpressing embryos at 5.3 hpf. The number of embryos is shown at the lower right corner of the panel. Animal pole views. Scale bars: 200 μm. (G) *sox32* expression in *nlacZ* or *dn smad2* mRNA overexpressing embryos at 5.3 hpf was measured by qPCR. Expression level of *nlacZ* overexpressing embryos is set as 1.0. **$p < 0.05$. Error bars represent the standard deviations of three independent experiments. (H, I) Cross sections of *nlacZ*- and *dn smad2*-overexpressing embryos; the cell membrane and nuclei were visualized by β-cat and DAPI staining, respectively at 4.7 hpf. Scale bars: 10 μm. (J, K) DNBs and DNCs in LMCs were measured in *nlacZ*- and *dn smad2*-overexpressing embryos at 4.7 hpf. n = number of nuclei examined.

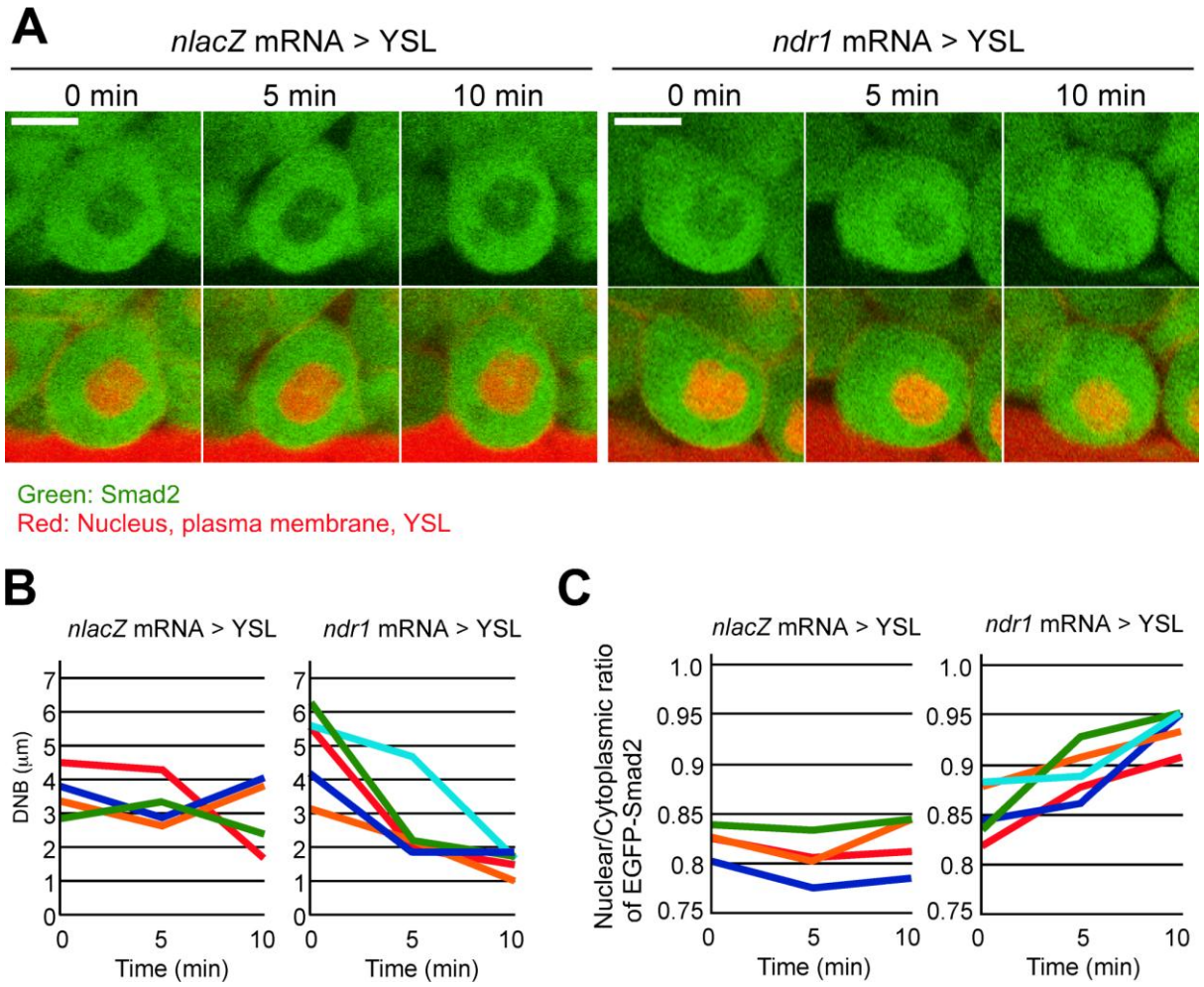

Figure 8. Visualization of Smad2 during nuclear movement

(A) Time-lapse confocal live imaging of EGFP-Smad2 in MMCs of *nlacZ* mRNA >YSL or *ndr1* mRNA>YSL embryos. Scale bars: 10 μm. (B, C) DNB values (B) and nuclear/cytoplasmic ratio of EGFP-Smad2 fluorescence (C) of 4 or 5 independent nuclei (represented by red, orange, green, dark blue, and light blue lines) in MMCs of *nlacZ* mRNA >YSL or *ndr1* mRNA>YSL embryos.

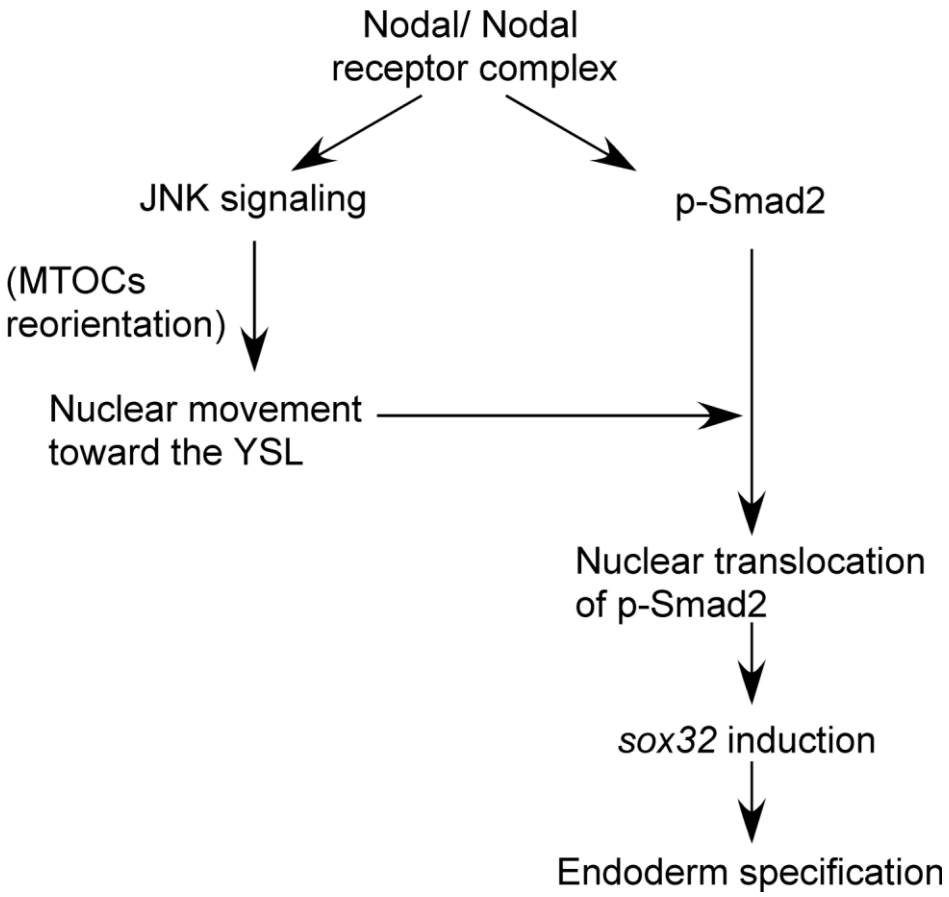

Figure 9. Proposed model for Nodal signaling pathways leading to endoderm specification in zebrafish LMCs

For discussion, see text.

Figure S1

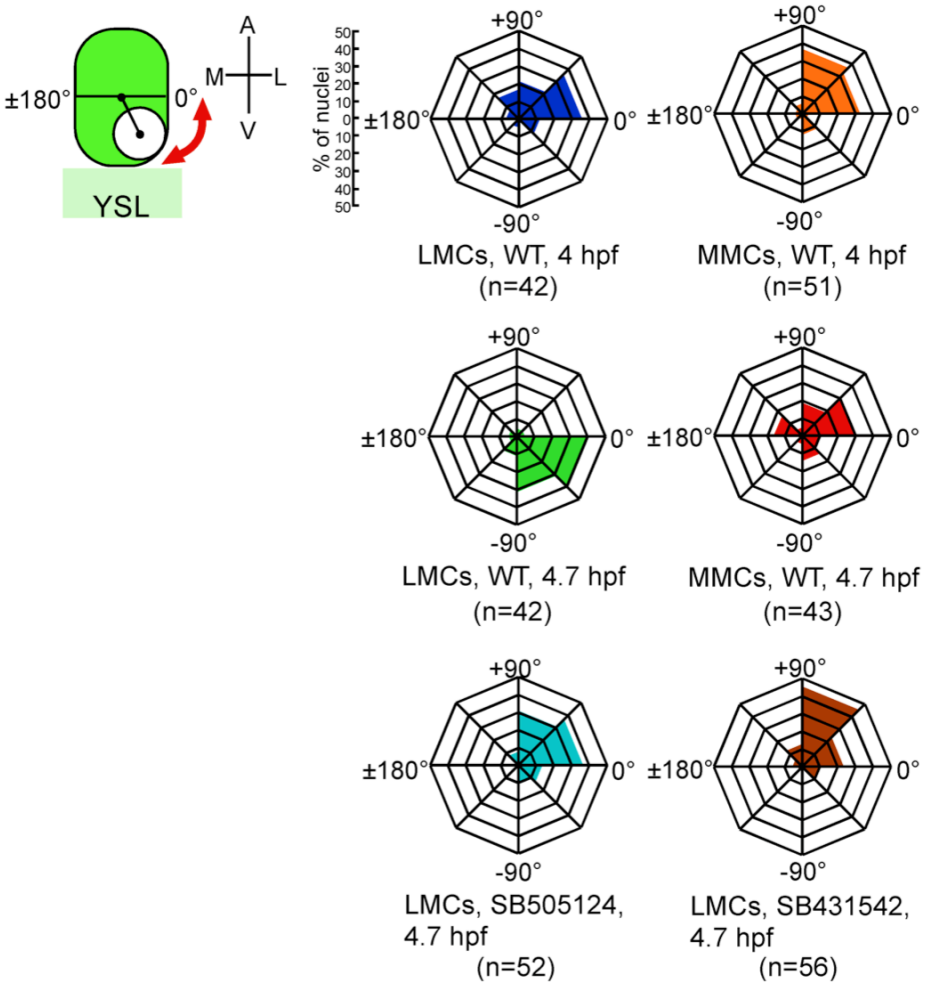

Figure S1. Nuclear positional changes in LMCs and MMCs between 4.0 and 4.7 hpf

Angles between the center of the cell and the nucleus relative to the medial-lateral axis were measured (red line). n = number of nuclei examined.

Figure S2

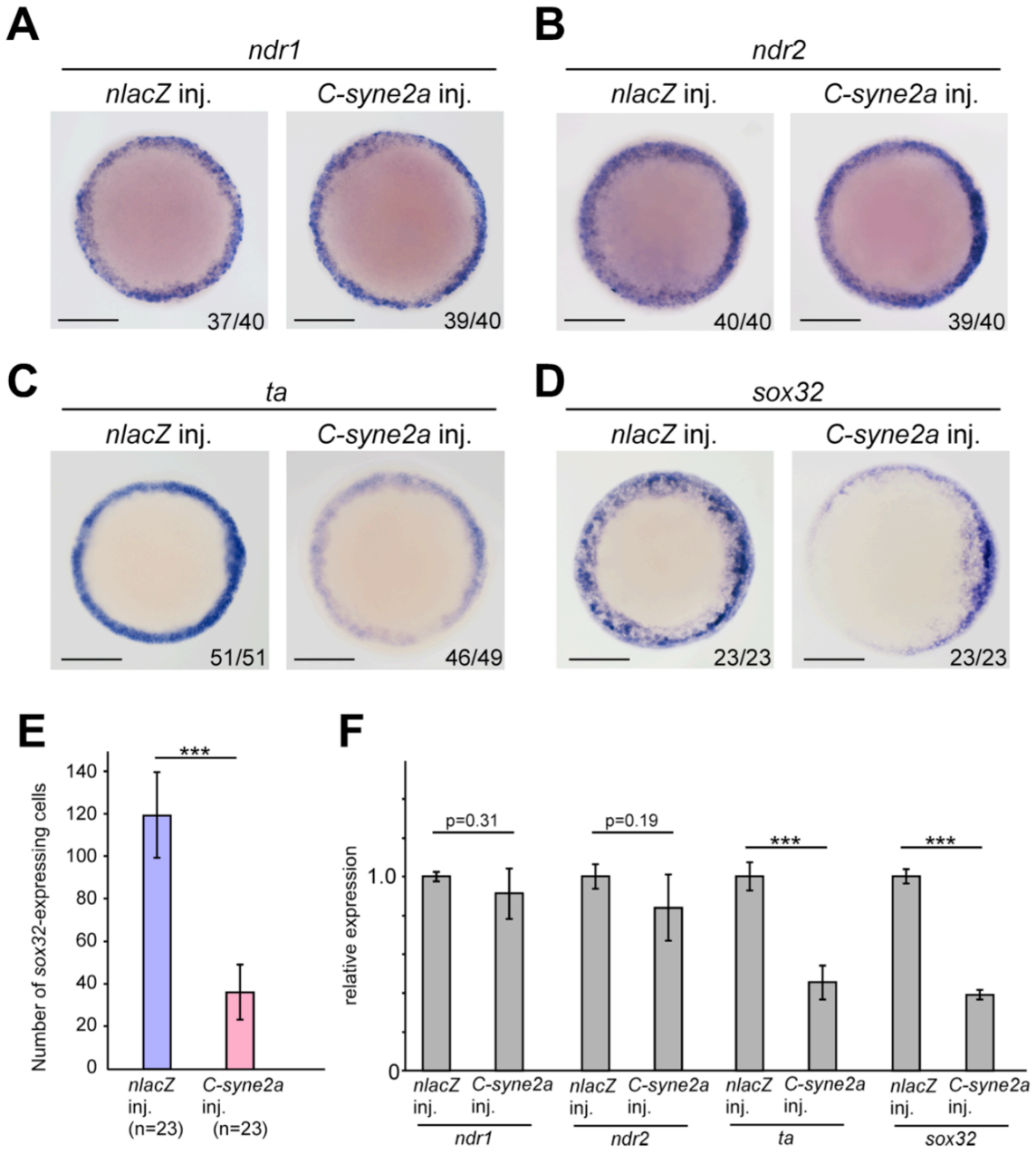

Figure S2. Expression of *ndr*, mesoderm, and endoderm genes in *C-syne2a*-overexpressing embryos

(A-D) Expression of *ndr1*, *ndr2*, *ta*, and *sox32* was examined by WISH in *nlacZ* or *C-syne2a* mRNA overexpressing embryos at 5.3 hpf. The number of embryos examined is shown at the lower right corner of each panel. Animal pole views. Scale

bars: 200 μm. (E) Number of *sox32*-expressing endodermal cells in *nlacZ*- or *C-syne2a*-overexpressing embryos at 5.3 hpf. n = number of embryos examined. ***$p < 0.001$. (F) Expression of *ndr1*, *ndr2*, *ta*, and *sox32* was examined by qPCR in *nlacZ* or *C-syne2a* mRNA-overexpressing embryos at 5.3 hpf. Error bars represent standard deviations of three or four independent experiments. ***$p < 0.001$.

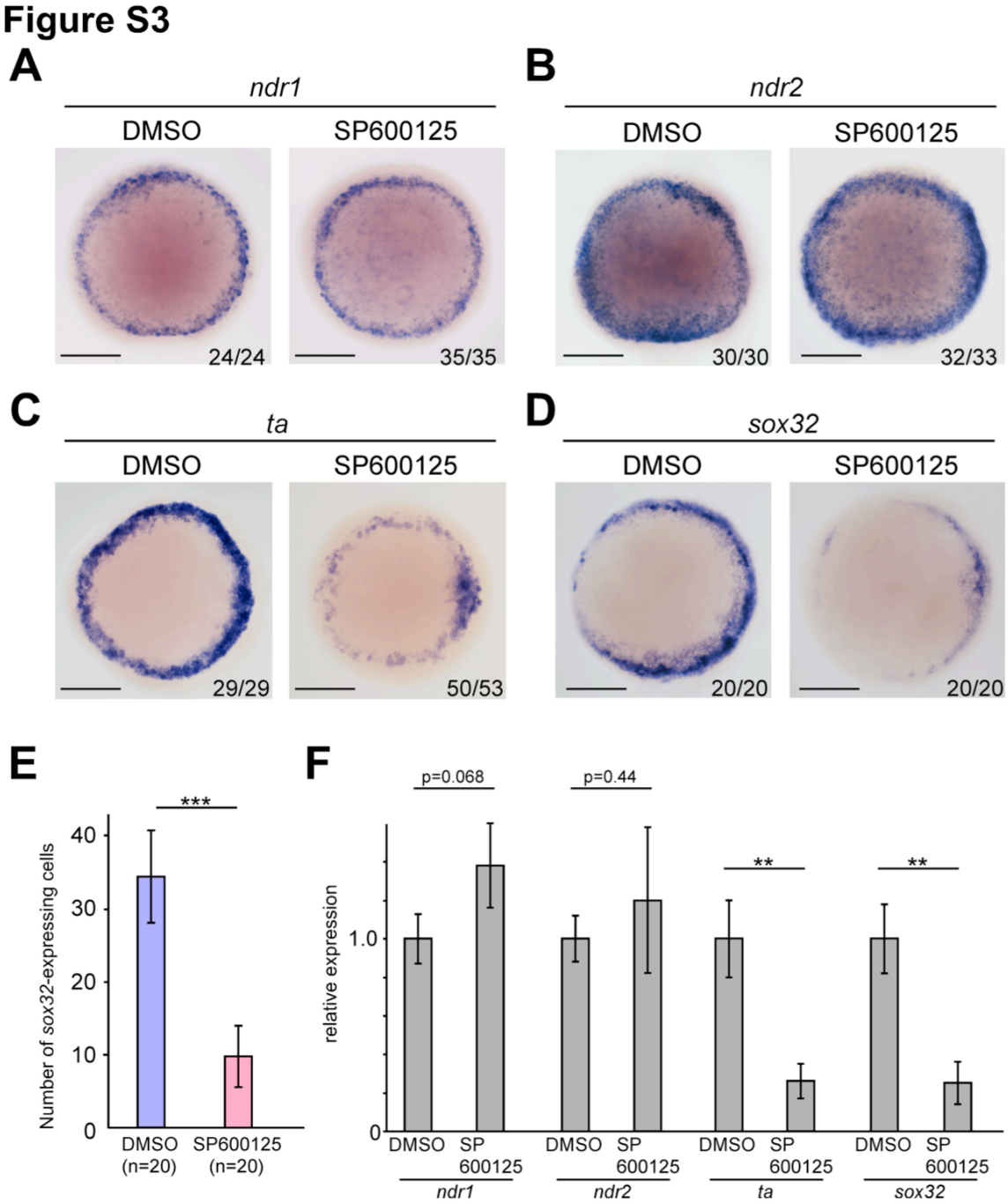

Figure S3. Expression of *ndr*, mesoderm, and endoderm genes in SP600125-treated embryos

(A-D) Expression of *ndr1*, *ndr2*, *ta*, and *sox32* was examined by whole-mount *in situ* hybridization in DMSO- or SP600125-treated embryos at 4.7 hpf. Number of embryos

examined is shown at the lower right corner of each panel. Animal pole views. Scale bars: 200 μm. (E) Number of *sox32*-expressing endodermal cell was counted in DMSO-, or SP600125-treated embryos. n = number of embryos examined. ***$p <$ 0.001. (F) Expression of *ndr1*, *ndr2*, *ta*, and *sox32* was examined by qPCR in DMSO- or SP600125-treated embryos at 4.7 hpf. Error bars represent standard deviations of three or four independent experiments. ***$p < 0.001$. ** $p < 0.05$.

Figure S4

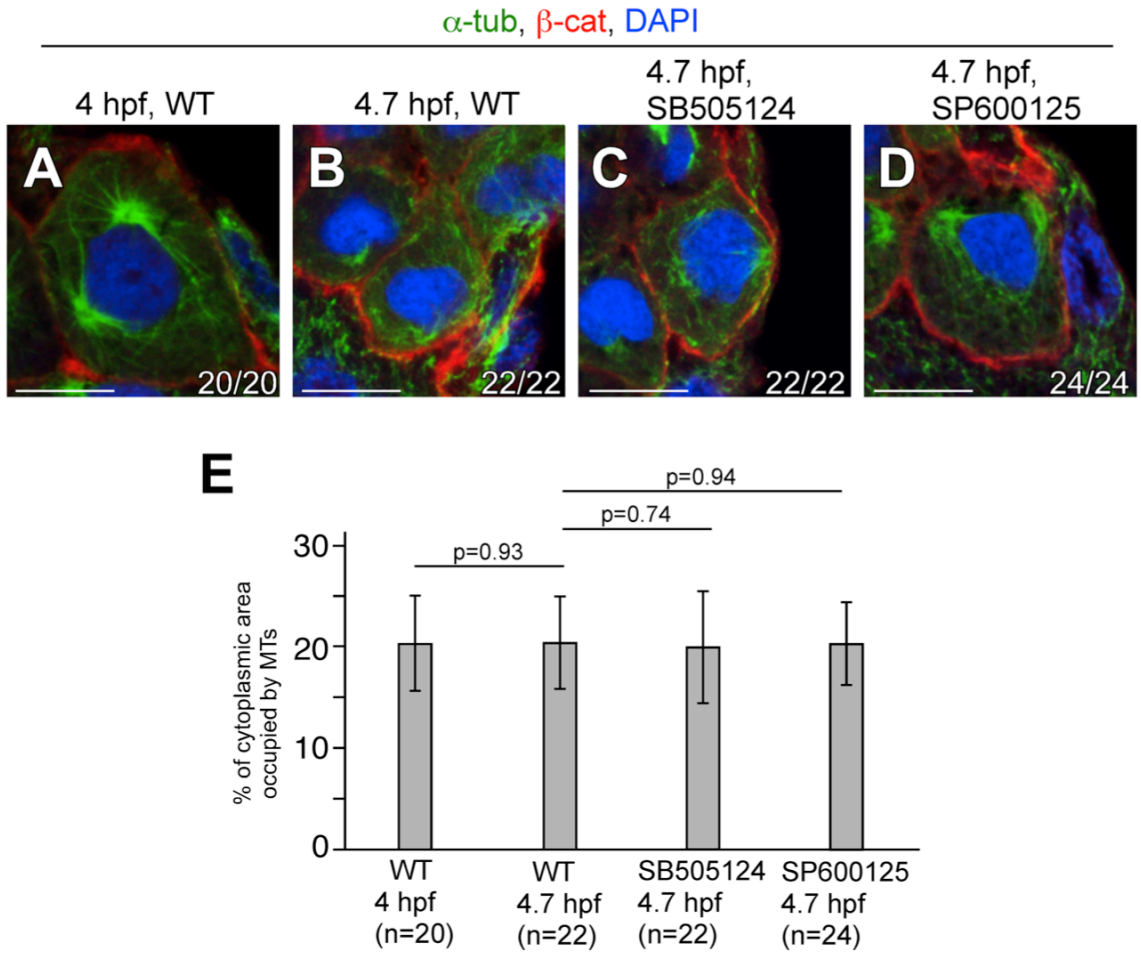

Figure S4. MT formation was not affected by inhibition of Nodal or JNK signaling

(A-D) Cross sections of WT, SB505124-, and SP600125-treated embryos; MTs, cell membrane, and nuclei were visualized by α-tubulin (α-tub), β-cat, and DAPI staining, respectively at 4.0 or 4.7 hpf. Number of nuclei examined is shown at the lower right corner of each panel. Scale bars: 10 μm. (E) Percentage of cytoplasmic area occupied by MTs in LMCs of WT, SB505124-, and SP600125-treated embryos.

Figure S5

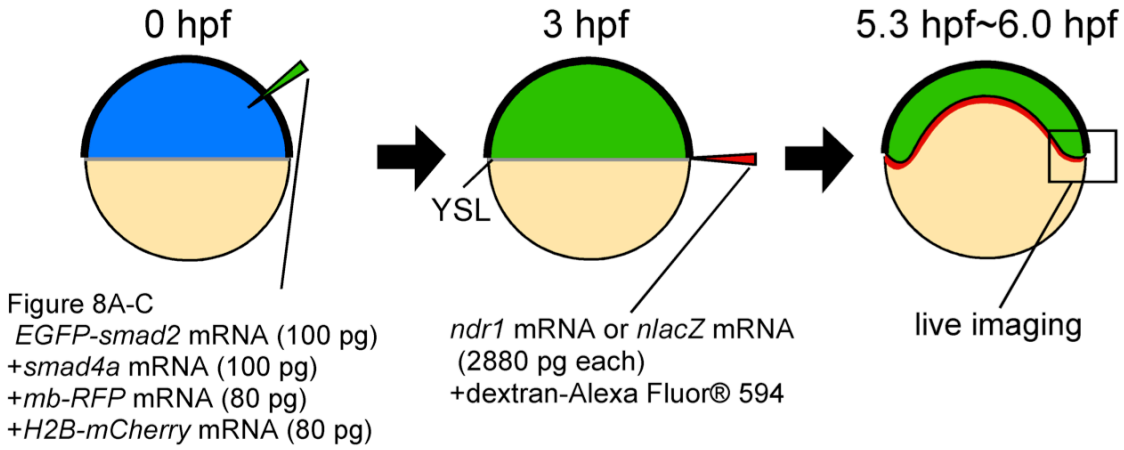

Figure S5. Experimental design of work presented in Figure 8

A mixture of *EGFP-smad2*, *smad4a*, *mb-RFP*, and *H2B-mCherry* mRNAs was injected into WT embryos at the one-cell stage. At 3 hpf, *ndr1* or *nlacZ* mRNA was injected with dextran-Alexa Fluor® 594 into the YSL, and confocal live images were captured at 5.3-6.0 hpf.

Movie S1

Time-lapse image of the nucleus in LMC between 4.0 and 4.7 hpf. A white dotted line indicate the boundary between the blastoderm and the YSL. Thick white lines indicate DNBs.

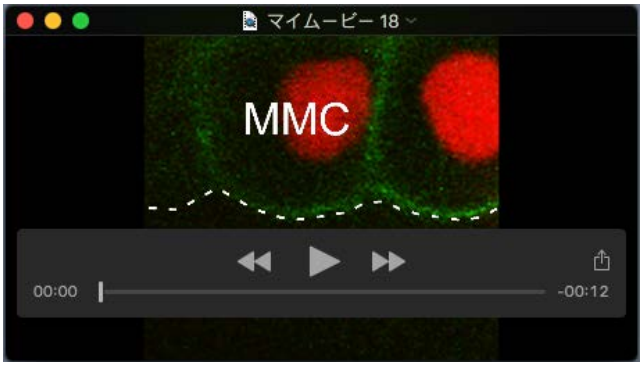

Movie S2

Time-lapse image of the nucleus in MMC between 4.0 and 4.7 hpf. A white dotted line indicate the boundary between the blastoderm and the YSL. Thick white lines indicate DNBs.